*Final Report*

# STUDY OF THE MECHANISMS OF FLUX PINNING IN TYPE-II SUPERCONDUCTORS

*Prepared for*

GEORGE C MARSHALL SPACE FLIGHT CENTER
NATIONAL AERONAUTICS AND SPACE ADMINISTRATION
HUNTSVILLE ALABAMA

CONTRACT NAS8-24816

## STANFORD RESEARCH INSTITUTE
Menlo Park, California 94025 · U S A

STANFORD RESEARCH INSTITUTE
Menlo Park, California 94025 · U.S.A.

# STUDY OF THE MECHANISMS OF FLUX PINNING IN TYPE-II SUPERCONDUCTORS

*By*   H  T  COFFEY  F  CHILTON, and  T  W  BARBEE  Jr

*Prepared for*

GEORGE C  MARSHALL SPACE FLIGHT CENTER
NATIONAL AERONAUTICS AND SPACE ADMINISTRATION
HUNTSVILLE, ALABAMA

Attention   DR  EUGENE URBAN

CONTRACT NAS8-24816

SRI Project 8043

*Approved*

ARYEH H  SAMUEL *Manager*
*Special Programs Group*

EDWIN M  KINDERMAN *Director*
*Physical Sciences (Applied Physics Laboratory)*

C  J  COOK *Executive Director*
*Physical Sciences Division*

CONTENTS

ILLUSTRATIONS

# ILLUSTRATIONS

ILLUSTRATIONS

TABLES

# INTRODUCTION

This final report includes work performed on the "Study of the Mechanisms of Flux Pinning in Type-II Superconductors," under NASA contract NAS8-24816. The work reported was performed during the first year of a project expected to be of two to three years duration During the course of this work, it became necessary to limit the program to the funds allocated for one year of effort.

The term "flux pinning" refers to the interaction of quantized vortices of magnetic flux (fluxoids) in type-II superconductors with defects in the superconducting sample This interaction restricts the motion of fluxoids in the sample and can pin them to the sites of defects. Since fluxoids are restricted in their motion, a gradient in the flux density results and a current density is established such that the pinning force equals the Lorentz force on the fluxoids

In materials without defects, a current density cannot be established. Thus, defects are introduced intentionally to obtain materials with currents useful for practical purposes. Generally, defects are introduced in superconductive alloy wires in the process of reducing them from ingot to wire size. Superconductive intermetallic compounds are produced generally at high reaction temperatures and normally contain many defects. Some degree of control over the defects introduced is possible in the metallurgical processing of these materials, but unfortunately at present there is no method of determining which defects are important in establishing a specific magnitude or characteristic of the resulting current density. Present materials were developed empirically.

1

The objective of this work was to develop a method of determining the effect of various types of defects on the current density and thereby specifying ways of making superconductors with properties appropriate to specific applications.

The fundamental property of defects used in this program was the change in the Ginzburg-Landau parameter $\varkappa$ associated with each type of defect. Knowing this change in $\varkappa$ and the distance over which the change occurs, the change in energy with distance, i e., the pinning force, can be determined

The program consisted of three parts    (1) development of a theoretical model capable of describing the interaction of fluxoids with specific types of defects, (2) determination of the distribution of $\varkappa$ in the superconductor using measured values of the specific heat capacity,* and (3) measurement of the distance between fluxoids (from which fluxoid forces can be determined) and determination of the underlying defect structure using electron microscopy. From (3) above, the relative numbers of defects of various types would be evaluated and from (2), the $\Delta\varkappa$ associated with each defect would be determined

Parts (1) and (2) above were completed successfully, but experimental difficulties were encountered in part (3) that prevented us from obtaining the data required to treat the entire flux pinning problem coherently and verifying the theoretical predictions.

---

* The specific heat measurements were made at Stanford University by Mr  Robert Zubeck and are being continued under the direction of Dr  T  H  Geballe.  These measurements, together with their interpretation, are expected to form the basis of Mr  Zubeck's Ph D. dissertation.

SUMMARY


Theoretical and experimental studies were made of the flux pinning mechanisms in type-II superconductors. A theoretical model based on the London theory was used to obtain trial functions for a variational calculation using the Ginzburg-Landau theory  The microscopic properties of fluxoids were calculated. The model was applied to the problem of flux pinning by (1) large defects having a $\varkappa$ gradient, (2) small normal regions or voids, and (3) small regions having $\varkappa$ values different from the bulk of the sample  The forces arising from these pinning mechanisms were related to the critical transport current and were found to provide reasonable approximations to experimental data  Item (3) above seems to be responsible for the peak effect in type-II superconductors.

Specific heat measurements were made on annealed and deformed pure niobium samples  Changes in the normal-superconducting transition induced by straining the samples were analyzed, yielding the distribution of $\varkappa$ and $T_o$ throughout the sample  The method developed should be valuable for the general analysis of defects in superconducting materials

Attempts were made to decorate fluxoids using the Bitter pattern technique and correlate the observed distributions with the underlying defect structures. Tight adhesion of the ferromagnetic powder to the sample prevented stripping the powder for observation in an electron microscope.

3

# THEORETICAL MODEL

## Introduction

Many properties of defect-free type-II superconductors have been described by Abrikosov,[1] Gorkov[2] and others based on the Ginzburg-Landau[3] theory of superconductivity. One of the major distinctions between the Ginzburg-Landau theory and the earlier London[4] theory of superconductivity is the spatial dependence of the order parameter, $\psi$, in the Ginzburg-Landau theory and its constancy in the London theory This difference affects the predicted behavior of the density of superconducting electrons in the vicinity of a boundary between normal and superconducting regions of the material. The London theory predicts a uniform condensation of electrons into the superconducting state while the Ginzburg-Landau theory predicts a condensation gradient of superconducting electrons over a distance characterized by the coherence distance $\xi$.

In their original paper, Ginzburg and Landau noted that in certain materials superconductivity would not be suppressed at the thermodynamic critical field, $H_c$, but would persist to a field $H_{c2} = \sqrt{2}\,\varkappa H_c$. The parameter $\varkappa$ is approximately $\lambda_L/\xi$ where $\lambda_L$ is the depth of penetration of a magnetic field in the London theory Abrikosov considered this phenomenon in more detail and discovered that for fields between $H_{c1} \leq H_c \leq \sqrt{2}\,\varkappa H_c \equiv H_{c2}$, quantized vortices of supercurrents occurred in these materials The condition for a material that can have these vortices is that $\varkappa$ be $\geq 1/\sqrt{2}$ These materials are referred to as type-II superconductors

Abrikosov found that in these vortices the current density vanishes at the center, reaches a peak value at a distance of approximately $\xi$ from the core, and decreased at larger radii  As a consequence of this behavior, the magnetic field is greatest at the center of the fluxoid. The flux $\varphi_0$ in these fluxoids is $h_c/2e$ or $2.07 \times 10^{-7}$ G - $cm^2$.

Although the Ginzburg-Landau theory describes these properties, it is mathematically difficult to use  The model to be presented here describes all these features in a mathematically tractable but approximate form.

## Formulation of the Model

De Gennes[5] and his coworkers developed a model of type-II superconductivity starting with the London equation

$$\text{CURL}(\lambda^2 \text{ CURL } \mathbf{h}) + \mathbf{h} = 0 \quad . \tag{1}$$

For a single fluxoid with cylindrical symmetry and $\lambda = \lambda_L$, the London penetration depth, equation (1) becomes

$$x^2 \frac{d^2 h}{dx^2} + x \frac{dh}{dx} - x^2 h = 0 \quad , \tag{2}$$

in terms of $x \equiv r/\lambda_L$  The solutions to equation (2) are the modified Bessel functions $K_0(x)$ and $I_0(x)$ which have the unphysical feature of a singular core  A  cutoff can be introduced by letting $\lambda$ be spatially dependent. This penetration depth is related to the superconducting order parameter, $\psi$, by $\lambda = \lambda_L/\psi$.

Now equation (1) becomes

$$x^2 \frac{d^2 h}{dx^2} + \left[ 1 + x\psi^2 \frac{d\psi^{-2}}{dx} \right] x \frac{dh}{dx} - x^2 \psi^2 h = 0 \tag{2$'$}$$

5

If

$$\psi = N \frac{x}{y} \tag{3}$$

where $y = (x^2 + \epsilon^2)^{\frac{1}{2}}$ and N and $\epsilon$ are field dependent variational parameters ($\epsilon$ for cutoff and N for normalization) then equation (2') becomes

$$y^2 \frac{d^2h}{dy^2} + y \frac{dh}{dy} - y^2 h = 0 \tag{2''}$$

Equation (2'') has the solution

$$h = C_1 N K_0 (Ny) + C_2 N I_0 (Ny) \tag{4}$$

Where $C_1$ and $C_2$ are constants (independent of position but not field)

By introducing a cutoff into the London equation, we have obtained trial functions for the order parameter, equation (3), and local magnetic induction, equation (4)  These can be introduced into the Ginzburg-Landau free energy to determine N and $\epsilon$ by a variational procedure.

We investigated the possibility of other forms for equations (3) and (4) in detail, including such families of solutions as h proportional to an arbitrary function multiplied by a Bessel function of arbitrary argument, series solutions, exponentials of arbitrary functions, and so forth  No other choice that we investigated gave tractable forms for $\psi$ and h, simultaneously

A solution can now be constructed that approximates an Abrikosov fluxoid by causing the current density to vanish on a circular boundary of radius R  This construction consists of approximating the hexagon on which the current actually vanishes by a circle  This approximation has been used previously by several authors[6,7,8]  We demand further that the flux contained inside the circle be the flux quantum $\varphi_0$.  These

6

conditions require that $dh/dx\big|_R = 0$ and $\int h \cdot ds = \varphi_o$   Consequently, the magnetic induction is given by $B = \varphi_o/\pi R^2$

Using these conditions, we find

$$h_z \equiv h(x) = \frac{N\varphi_o}{2\pi\lambda_L^2 \epsilon} \frac{\gamma(R,y)}{\beta(R,\epsilon)} \tag{5}$$

$$J_\theta \equiv J(x) = \frac{N\varphi_o c}{8\pi^2 \lambda_L^3 \epsilon} \psi \frac{\beta(R,y)}{\beta(R,\epsilon)} \tag{6}$$

$$A_\theta \equiv A(x) = -\frac{\varphi_o}{2\pi\lambda_L \epsilon} \frac{y}{x} \frac{\beta(R,y)}{\beta(R,\epsilon)} + \frac{N\varphi_o}{2\pi r} \tag{7}$$

where

$$\gamma(R,y) = I_1(Ny_R)K_o(Ny) + K_1(Ny_R)I_o(Ny) \tag{8}$$

and

$$\beta(R,y) = I_1(Ny_R)K_1(Ny) - K_1(Ny_R)I_1(Ny) \tag{9}$$

and

$$y_R = (R^2/\lambda_L^2 + \epsilon^2)^{\frac{1}{2}} \tag{10}$$

Finally, it is noted that

$$J = -\frac{c}{4\pi\lambda_L^2} \psi^2 \left[ A - \frac{\varphi_o}{2\pi r} \right] \tag{11}$$

7

## London Free Energy

The usual form of the Lagrange energy density in the London theory is

$$L = \frac{1}{8\pi} [h^2 + (dh/dx)^2]$$  (12)

Writing equation (1) in its usual form, the equation for the local magnetic field is given by

$$\frac{d^2h}{dx^2} + \frac{1}{x}\frac{dh}{dx} - h = 0$$  (13)

and has the solution

$$h = D_1 K_o(x) + D_2 I_o(x)$$  (14)

At $x = 0$, both $h$ and $dh/dx$ become infinite leading to an infinite energy density at the core of a fluxoid  The present model can be obtained from the formal transformation of $x$ into $Ny$  In this case, the Lagrange energy is

$$L = \frac{1}{8\pi} [h^2 + (dh/d(Ny))^2]$$  (15)

which has the same form as equation (12)  At $x = 0$, however, the arguments of the K functions become $N\epsilon$ and the energy remains finite.  The free energy per unit length of fluxoid is obtained by integrating the free energy density over the cross section of the fluxoid, resulting in the simple expression

$$\frac{F}{Z} = \frac{\varphi_o h(N\epsilon)}{8\pi}$$  (16)

8

## Ginzburg-Landau Free Energy

Since a functional form of $\psi(x)$ has been assumed and a corresponding expression for $h(x)$ has been calculated, it is possible to use these to obtain an approximate solution of the Ginzburg-Landau equations  The Ginzburg-Landau free energy will be minimized with respect to the parameters N and $\varepsilon$ to yield the values of these parameters which give the lowest energy

The Ginzburg-Landau free energy density has the functional form

$$F_{SH} - F_{NO} = -\frac{H_c^2}{4\pi}\left[|\psi|^2 - \frac{1}{2}|\psi|^4\right] + \frac{h^2}{8\pi} + \frac{1}{2m}\left|-i\hbar\nabla\psi - \frac{e^*}{c}\underset{\sim}{A}\psi\right|^2 \quad (17)$$

from which the following two equations can be derived

$$\nabla^2\psi + \frac{\varkappa^2}{\lambda^2}\left(1 - \frac{A^2}{2\lambda^2 H_c^2}\right)\psi - \frac{\varkappa^2}{\lambda^2}\psi^3 = 0 \quad (18)$$

$$\underset{\sim}{J} = -\frac{c}{4\pi\lambda^2}\left[\psi^2\underset{\sim}{A} + \frac{i\varphi_0}{4\pi}(\psi^*\nabla\psi - \psi\nabla\psi^*)\right] \quad . \quad (19)$$

Cylindrical symmetry and single-valuedness have been assumed, implying that $\psi$ can be written in the form $\psi = |\psi|e^{i\theta}$  Substituting this $\psi$ with $|\psi| = (Nx/y)$ into equation (19), we find that equation (19) is identical to equation (11) if the expressions for j and A from equations (6) and (7) are used

Substituting h and $\psi$ into equation (17) and letting $\varkappa = \lambda/\xi$, $Hc = \varphi_0/2\sqrt{2}\pi\lambda\xi$, and $H_{c2} = \varphi_0/2\pi\xi^2$, the free energy in this approximation can be shown to be

$$F_{SH} - F_{NO} = -\frac{H_c^2}{4\pi}\left[\left(\frac{Nx}{y}\right)^2 + \frac{1}{2}\left(\frac{Nx}{y}\right)^4\right] + \frac{1}{8\pi}\left[h^2 + \left(\frac{dh}{d(Ny)}\right)^2\right] + \frac{H_c^2}{8\pi}\left(\frac{Ne^2}{\varkappa y^3}\right)^2 \quad .$$

$$(20)$$

9

It is seen immediately that the energy of the modified London model [equation (15)] is only one part of the Ginzburg-Landau free energy The first term is the condensation energy and the last term is a part of the $\nabla\psi\nabla\psi^*$ term.

Integrating equation (20) over the cross section of a fluxoid and dividing by the cross-sectional area, the free energy per unit volume becomes

$$\frac{8\pi}{H_c^2}\left(F_{SH} - F_{NO}\right) = -2N^2\left(1 - \frac{N^2}{2}\right) + \frac{2\varkappa^2\epsilon^2 B}{H_{c2}}N^2(1 - N^2)\ln(y_R/\epsilon)$$

$$+ \frac{Bh(N\epsilon)}{H_c^2} + \frac{N^2}{y_R^2}\left[N^2\epsilon^2 + \frac{1}{\varkappa^2}\left(1 + \epsilon^2/y_R^2\right)\right] \qquad (21)$$

The external magnetic field $H = 4\pi(\partial/\partial B)(F_{SH} - F_{NO})_H$ can be obtained from equation (21)

$$\frac{H}{H_{c2}} = \frac{N^2\epsilon^2}{2}(1 - N^2)\left[\ln(y_R/\epsilon) - \frac{H_{c2}}{\varkappa^2 y_R^2 B}\right] + \frac{N^2 H_{c2}}{2\varkappa^4 y_R^4 B^2}\left[N^2\epsilon^2 + \frac{1}{\varkappa^2}\left(1 + \frac{2\epsilon^2}{y_R^2}\right)\right]$$

$$+ \frac{H_{c2}}{2\varkappa^4\epsilon^2 y_R^4 B\beta^2(R,\epsilon)} + \frac{N\gamma(R,\epsilon)}{2\varkappa^2\epsilon\beta(R,\epsilon)} \qquad (22)$$

Finally, the Gibbs energy is given by

$$G_{SH} - G_{NH} = F_{SH} - F_{NO} - \frac{BH}{4\pi} + \frac{H^2}{8\pi} \qquad (23)$$

As $B \to 0$, N approaches 1 and $y_R$, $\beta$ and $\gamma$ approach infinity Under these conditions, the first and third terms of equation (22) vanish. The limit as $B \to 0$ of the remaining two terms define the lower critical field $H_{c1}$

10

$$\frac{H_{c1}}{H_{c2}} = \frac{1}{8} \left( \epsilon^2 + 1/\varkappa^2 \right) + \frac{K_0(\epsilon)}{2\varkappa^2 \epsilon K_1(\epsilon)} \qquad . \qquad (24)$$

In this limit, the minimization procedure indicates that $\epsilon^2$ approaches $2/\varkappa^2$ yielding

$$\frac{H_{c1}}{H_{c2}} + \frac{3}{8\varkappa^2} + \frac{K_0(\sqrt{2}/\varkappa)}{2\sqrt{2}\varkappa K_1(\sqrt{2}/\varkappa)} \qquad (25)$$

Results of Model

It was found that when N and $\epsilon$ were varied, the lowest energy at low fields was obtained when $\psi$ slightly exceeded unity   For this reason, the physically realistic condition that $\psi$ be less than or equal to one was imposed.  Some of the parameters were evaluated for several values of $\varkappa$, but detailed results are given here only for $\varkappa = 5$.  These results are shown in Figures 1 through 5.

The average Gibbs energy per unit volume of the specimen is shown in Figure 1 as a function of the magnetic induction $B/H_{c2}$.  The magnetization $-4\pi M/H_{c2}$ was obtained numerically from equation $(22)$ by choosing a value of $B/H_{c2}$ and calculating $H/H_{c2}$   The results of this calculation are shown in Figure 2 where they are compared with the Abrikosov magnetization[1] given by

$$-4\pi M/H_{c2} = \frac{1 - H/H_{c2}}{1.16(2\varkappa^2 - 1)} \qquad . \qquad (26)$$

The difference between the local magnetic induction, $h(x)/H_{c2}$, and the average induction $B/H_{c2}$ is shown in Figure 3.  The local current density $j(x)$ inside the fluxoid, normalized by $cH_c/4\pi\lambda$, the London

11
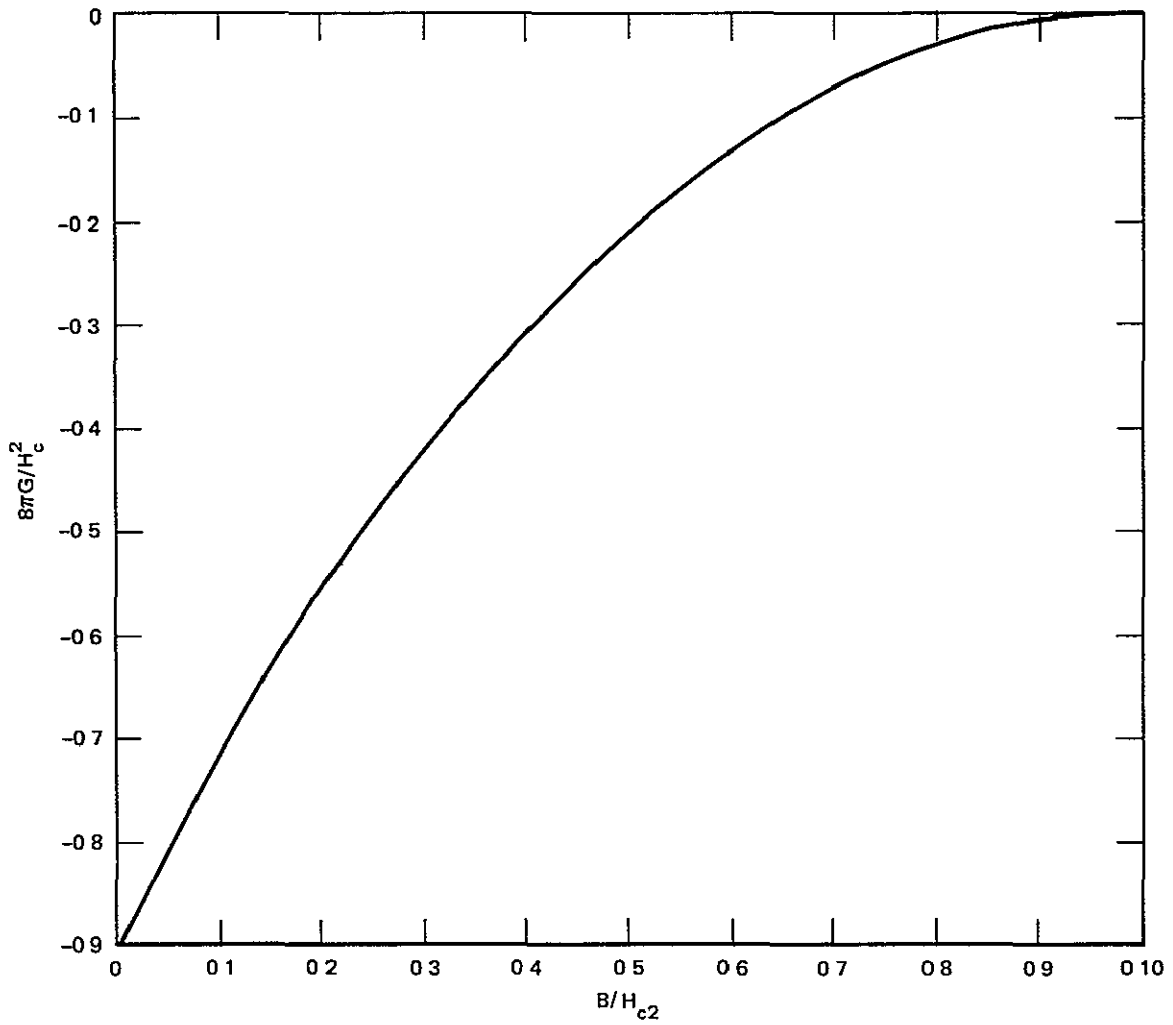
TA-8043-20

FIGURE 1    AVERAGE GIBBS ENERGY PER UNIT VOLUME VERSUS MAGNETIC
INDUCTION, $\kappa = 5$
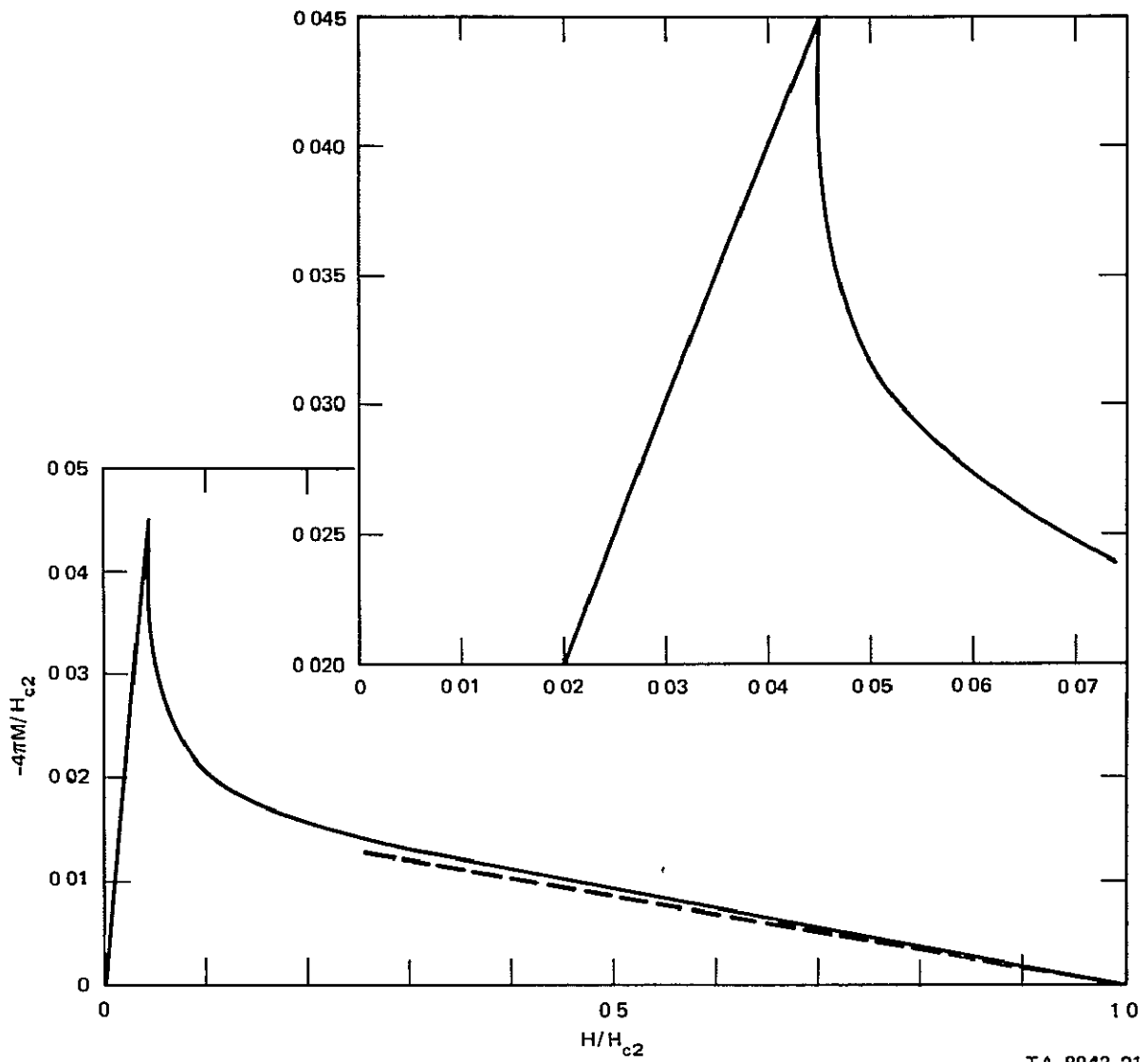
FIGURE 2    MAGNETIZATION, $-4\pi m/H_{c2}$    VERSUS $H/H_{c2}$ FOR $\kappa = 5$    The broken line is the Abrikosov prediction

13
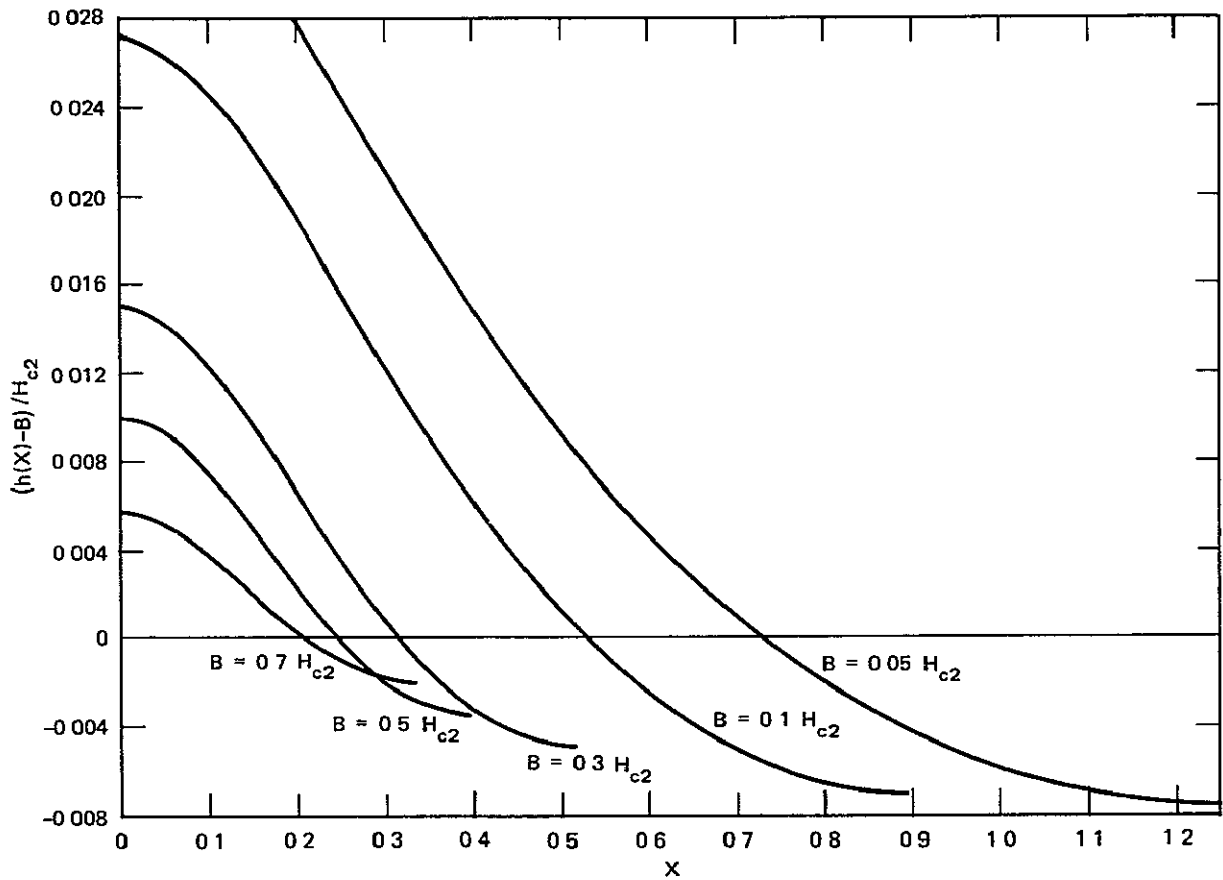
TA-8043-9

FIGURE 3   DIFFERENCE BETWEEN THE LOCAL MAGNETIC INDUCTION IN A FLUXOID
AND THE AVERAGE INDUCTION IN THE SAMPLE FOR VARIOUS VALUES
OF THE AVERAGE INDUCTION

14

TA–8043–8
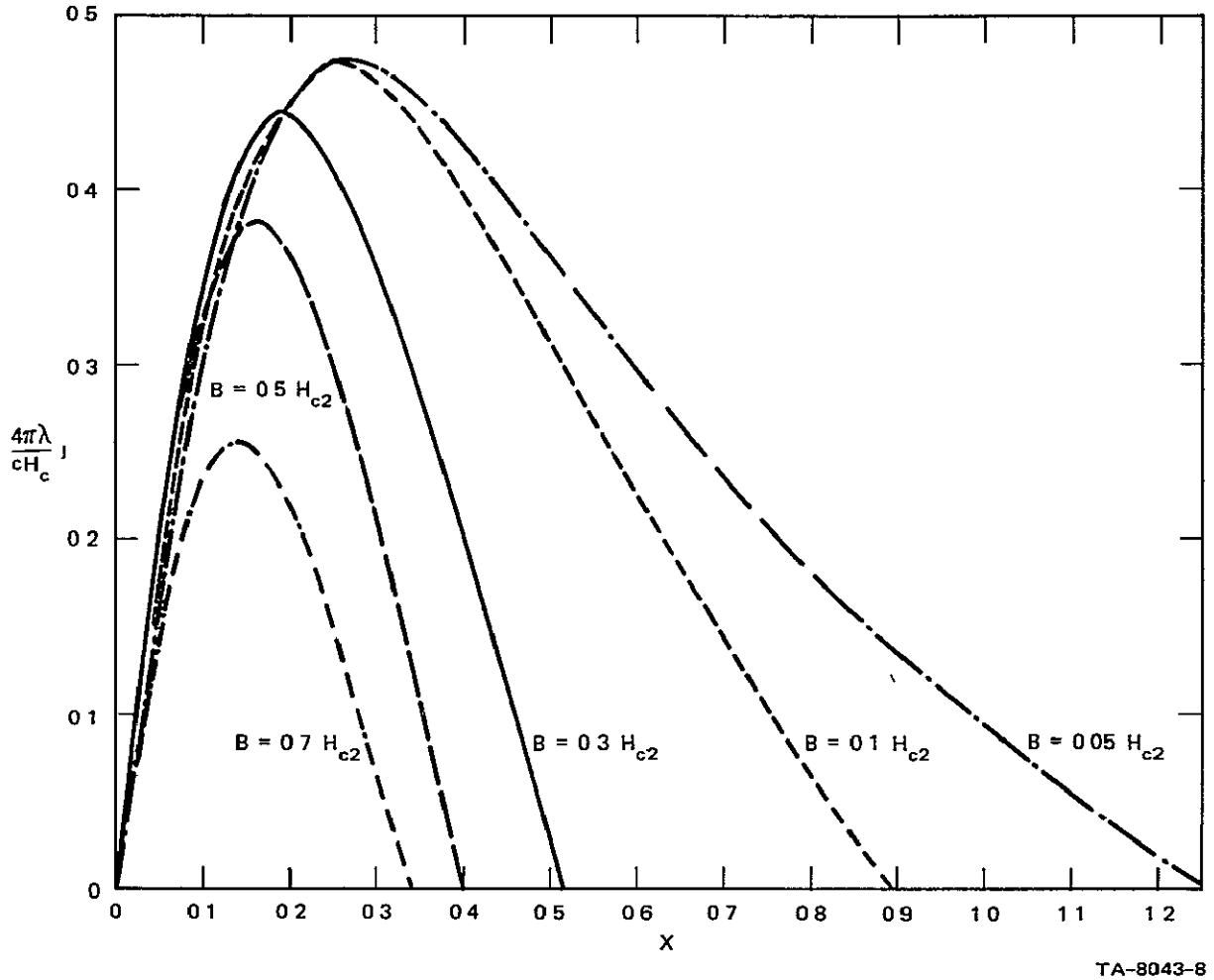
FIGURE 4    RATIO OF CURRENT DENSITY TO LONDON CRITICAL CURRENT DENSITY,
$cH_c/4\pi\lambda$ AS A FUNCTION OF POSITION INSIDE A FLUXOID FOR VARIOUS
VALUES OF THE MAGNETIC INDUCTION, $\kappa = 5$

TA-8043-7
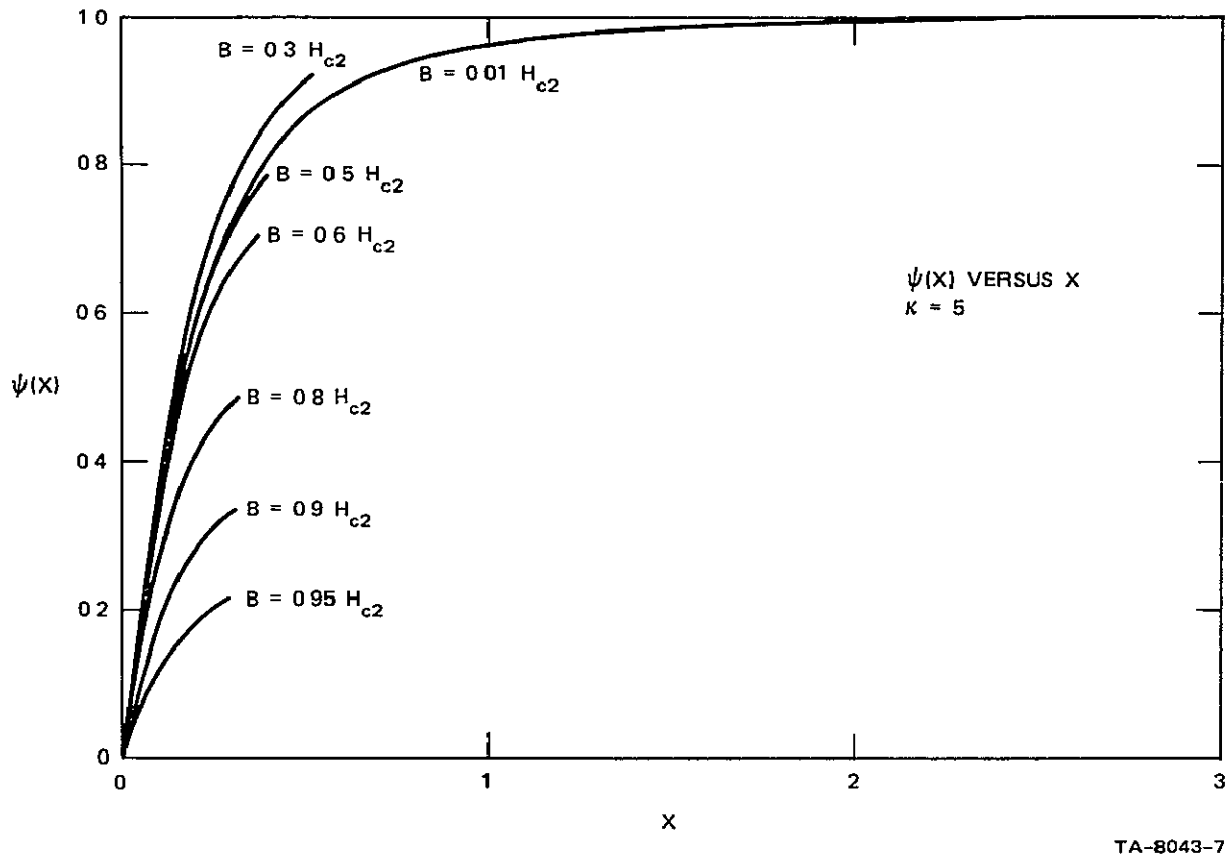
FIGURE 5    VARIATION OF THE ORDER PARAMETER, $\psi(\chi)$ WITH POSITION AND
MAGNETIC INDUCTION FOR $\kappa$ = 5


critical current density, is shown in Figure 4, the order parameter

$\psi(x)$ is shown in Figure 5.  A list of parameters applicable to the case

$\varkappa = 5$ is given in Table 1.


Pinning of Fluxoids

It is generally agreed that the pinning of fluxoids in supercon-
ductors is caused by imperfections in the superconducting sample   The
variety of imperfections in metals is quite diverse, ranging from simple
defects such as vacancy-interstitial pairs to grain boundaries, precipi-
tates, and composition variations in alloys.  Undoubtedly each of these
contributes to some extent to the total pinning force exerted on the

Table 1

PARAMETERS FOR $\varkappa = 5$

| $B/H_{c2}$ | $H/H_{c2}$ | $-4\pi M/H_{c2}$ | $8\pi G/H_c^2$ | $\epsilon^2$ | N |
|---|---|---|---|---|---|
| 0 005 | 0 04530 | 0 04030 | - 0 8973 | 0.082 | 1.0025 |
| 01 | 04627 | 03627 | -.8936 | 089 | 1 0055 |
| 02 | .05104 | 03104 | -.8777 | 091 | 1 0113 |
| .05 | 07389 | .02389 | - 8167 | 095 | 1 0292 |
| .1 | 1192 | 01924 | -.7206 | 094 | 1 0571 |
| 2 | 2152 | 01525 | - 5575 | 083 | 1 0668 |
| .3 | 3128 | 01282 | -.4209 | .0736 | 1 0378 |
| 5 | .5088 | 008849 | - 2092 | 0575 | 0.9126 |
| 6 | 6070 | 006983 | - 1314 | .0515 | 0 8239 |
| 7 | .7051 | 005151 | -.07183 | 0465 | 0.7157 |
| 8 | 8033 | 003333 | -.03016 | 0425 | 0.5813 |
| 9 | 9015 | .001525 | - 006315 | 0392 | 0 3962 |
| 95 | 9506 | 00621 | -.001049 | 0377 | 0 2537 |

fluxoid lattice. Since so many different types of imperfections are present in commonly available materials, it is difficult to determine which imperfections contribute most to the total pinning force by measuring macroscopic quantities such as the critical current or the magnetization of the sample

Experimentally, attempts have been made to reduce the number of types of pinning centers by carefully controlling the metallurgical preparation of the samples  Numerous experiments of this type have introduced known amounts of precipitates in a host matrix, known amounts of radiation induced defects in well annealed samples, and known amounts and sizes of grain and subgrain boundaries [9-20]

Theoretical treatments of pinning are complicated by the inability
to describe fluxoids that are nonsymmetric  Thus, if a fluxoid is posi-
tioned over a region of the sample in which the metallurgical, and there-
fore the superconductive, properties vary significantly, the properties
of the fluxoid cannot be described adequately.  For this reason, valid
calculations can only be made if the change in superconductive properties
occurs over a distance that is large compared to the fluxoid dimensions,
or if the change in properties occurs over a region that is small enough
compared with the fluxoid that the fluxoid geometry can be assumed to be
unperturbed  Imperfections intermediate in size between these limits
cannot be treated at present.  These two limiting cases are considered
in the following discussion

Consider first the effect of a large imperfection such as a cell
wall, grain boundary, or precipitate  Such imperfections range in size
from about $2 \times 10^{-6}$ cm to $2 \times 10^{-5}$ cm or larger depending on the purity
and thermomechanical history of the sample  (We will use the example of
a cell wall or grain boundary to which defects and impurities have mi-
grated )  These imperfections lead to a reduction in the electron mean-
free-path, an increase in the resistivity, and consequently to an in-
crease in $\varkappa$ according to the relation[21]

$$\varkappa = \varkappa_o + \varkappa_\ell = \varkappa_o + 7.5 \times 10^3 \gamma_e^{\frac{1}{2}} \rho_n \qquad (27)$$

where $\varkappa_o$ is the value of $\varkappa$ in the defect free portion of the sample, $\gamma_e$
is the electronic specific heat, and $\rho_n$ is the normal state resistivity

Assume that through the cell wall of width 2w the value of $\varkappa$ is
triangular in shape, increasing from 0 to w and decreasing from w to 2w.
Thus, $d\varkappa/dx$ is constant from 0 to w and the pinning force associated
with this gradient in $\varkappa$ is

18

$$\frac{f_p}{V} = \frac{\partial G}{\partial \varkappa}\frac{\partial \varkappa}{\partial x} \approx \frac{\partial G}{\partial \varkappa}\frac{\Delta \varkappa}{W} \qquad (28)$$

Letting the total length of imperfections perpendicular to the force be s, and the length of the fluxoid parallel to the imperfection be $\ell$, the volume over which the force acts is sw$\ell$ and the pinning force on the imperfection is

$$f_p = 2\frac{\partial G}{\partial \varkappa}\Delta\varkappa s\ell \qquad (29)$$

where the force on each side of the wall has been included   It will be shown later that $\partial G/\partial \varkappa$ is negative for an increase in $\varkappa$, and therefore the force is attractive on both sides of the wall, drawing fluxoids into the wall

Since the width of the wall does not occur in the final expression, it seems at first sight that only the change in energy between 0 and w or w and 2w is important.  However, this formulation is only valid if w > 2R and $d\varkappa/dx$ is small, otherwise, the energy of the fluxoid cannot be calculated. The radius of fluxoids is smallest at high fields and the calculation is most applicable   At low fields, the radius increases and fluxoids are more likely to encounter regions of widely varying $\varkappa$   Since a gradient in $\varkappa$ is assumed to exist only in the cell wall, a force is excited and a current flows only in this part of the sample

The current density in the layer w is found by equating the pinning force $f_p$ and the Lorentz force $jB/c$.

$$J = cf_p/B \qquad (30)$$

The average current density in the sample is

$$J = cf_p sw/BA \qquad (31)$$

19

where A is the cross-sectional area of the sample and sw/A is the fraction of the sample in which the current actually flows

The field dependence of $f_p$ arises from $\partial G/\partial \varkappa|_H$ which was obtained by numerical differentiation and is shown in Figure 6 for $\varkappa = 5$  The same figure shows the result of differentiating the Abrikosov energy under the same conditions.  The curves were not extended below $B/H_{c2} = 0\ 1$ due to numerical problems with the present calculation and the inapplicability of the Abrikosov energy at low values of $B/H_{c2}$  Neither curve goes to zero at $B = 0$ as might be inferred from the curves shown  The Abrikosov result can be shown to be
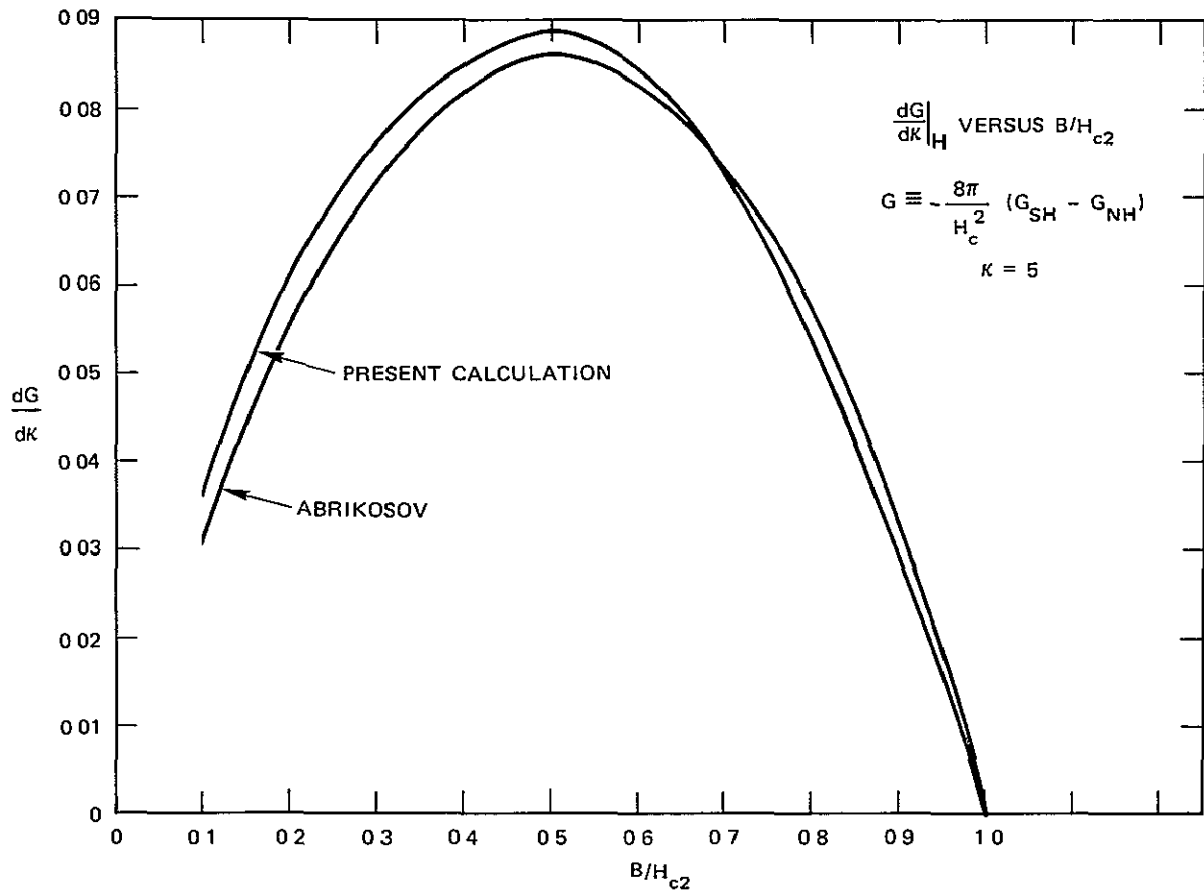


FIGURE 6    PARTIAL DERIVATIVE OF THE AVERAGE GIBBS ENERGY WITH RESPECT TO
$\kappa$ AS A FUNCTION OF THE MAGNETIC INDUCTION

20

$$\frac{8\pi}{H_c^2}\frac{\partial G}{\partial \varkappa} = -4\varkappa \frac{(1 - H/H_{c2})}{(2\varkappa^2 - 1)^2 \beta}\left(2\varkappa^2 \frac{H}{H_{c2}} - 1\right) \qquad (32)$$

where $\beta = 1 16.$[22]

For large values of $\varkappa$, this varies approximately as

$$\frac{8\pi}{H_c^2}\frac{\partial G}{\partial \varkappa} \approx -\frac{2H/H_{c2}(1 - H/H_{c2})}{1 16\varkappa} \qquad (33)$$

Using this approximation, the average current density in the sample is

$$J = -\frac{cH_c^2 S^2 w\ell\Delta\varkappa}{3.32\pi AH_{c2}}\frac{H}{\varkappa}\frac{H}{B}\left(1 - \frac{H}{H_{c2}}\right) \qquad (34)$$

The form of this current density is shown in Figure 7

To determine the effect of small defects on the pinning force, it is necessary to know the distribution of the Gibbs energy inside a fluxoid   This is obtained using equations (20) and (23) with B replaced by the local induction $h(x)$ in the latter equation.   In this case,

$$G_{SH} - G_{NH} = -\frac{H_c^2}{4\pi}[\psi^2(x) - \psi^4(x)/2] + \frac{(H - h(x))^2}{8\pi} + \frac{H_c^2}{4\pi}\left(\frac{Ne^2}{\varkappa y^3}\right)^2 \qquad (35)$$

This energy density per unit volume is shown in Figure 8 as a function of $x\lambda/R$ with $B/H_{c2}$ as a parameter.   It is surprising and previously un-recognized that although the average energy density in the fluxoid is negative (see Figure 1), the local energy density can be positive and quite large.   From the shape of these curves, it is seen that if  a small normal region exists inside the fluxoid, the largest amount of energy will be gained when this normal region lies at the center of the
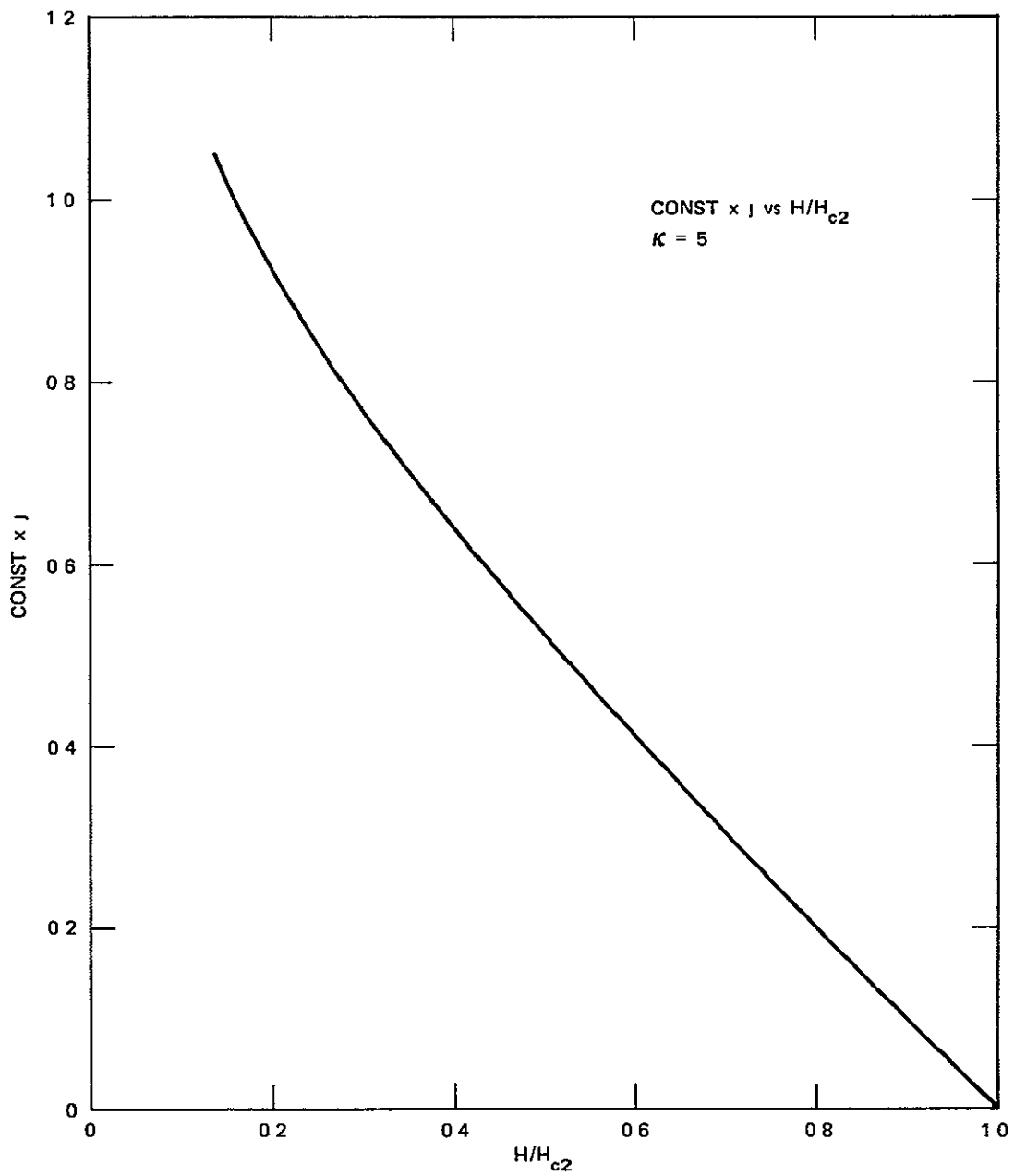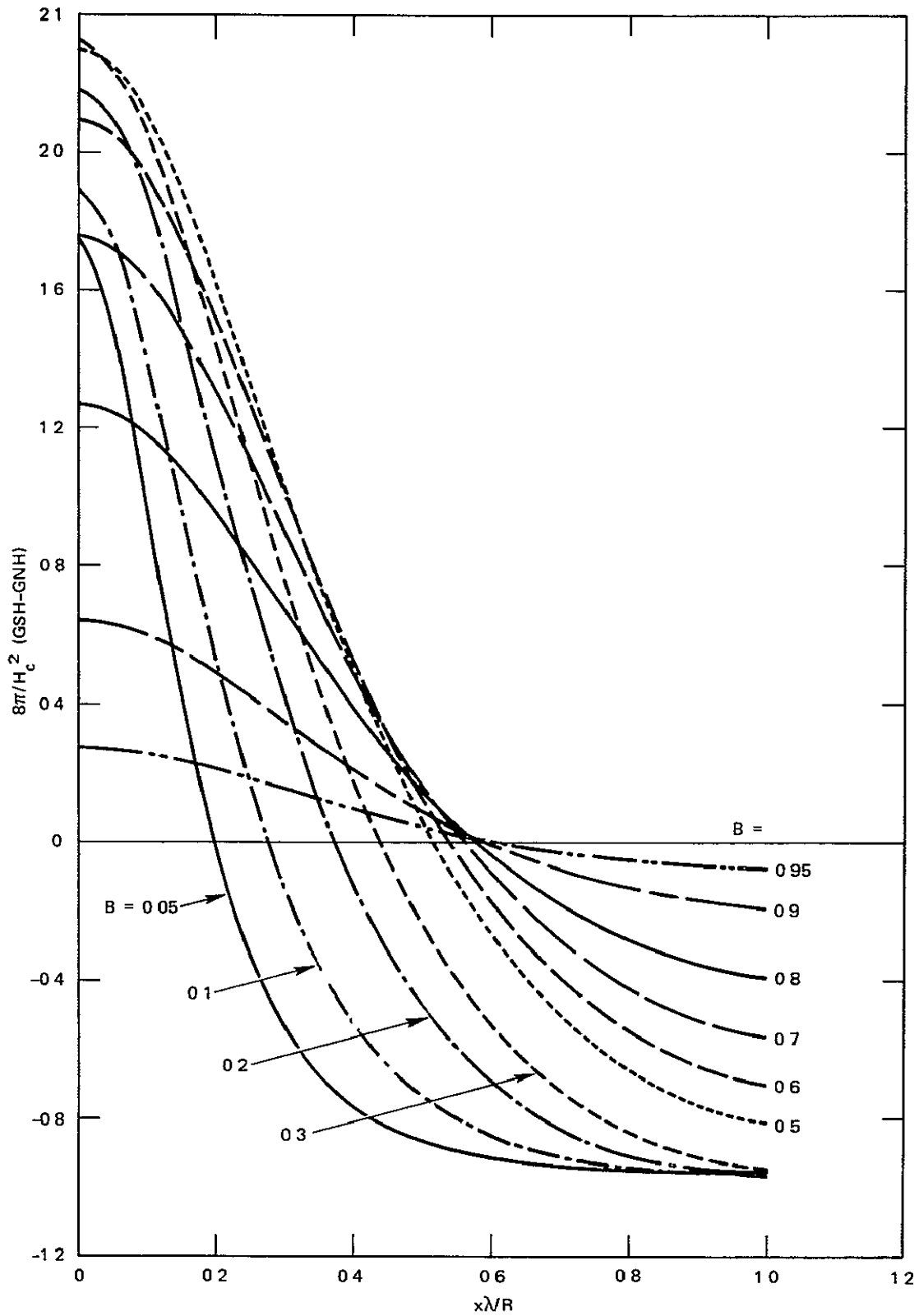
21

CONST $\times$ j vs $H/H_{c2}$
$\kappa = 5$

FIGURE 7   FORM OF THE CRITICAL CURRENT DENSITY WHEN PINNING IS CAUSED
BY LONG RANGE VARIATIONS IN $\kappa$ (See equation 34)

FIGURE 8    VARIATION OF THE GIBBS ENERGY AS A FUNCTION OF POSITION
INSIDE A FLUXOID FOR VARIOUS VALUES OF THE MAGNETIC
INDUCTION, $\kappa$ = 5 (See equation 35)

23

fluxoid   The slope of these curves gives the pinning force per unit
volume of normal inclusion in the fluxoid as a function of position and
magnetic induction.   The maximum slope, or the maximum force per unit
volume, does not occur at the center of the fluxoid but at some distance
from the center   To calculate the actual force, $\lambda$ and $H_c$ must be known
We choose, for illustrative purposes, the self-consistent parameters
$H_c = 2 \times 10^3$ Oe and $\lambda = 7\ 5 \times 10^{-6}$ cm from which it follows that
$\xi = 1.5 \times 10^{-6}$ cm, $H_{c2} = 14.6$ kOe, and $H_{c1} = 659$ Oe   In this case, the
maximum pinning force per unit volume of normal inclusion is shown in
Figure 9

To obtain the current density, it is necessary to know not only the
force on a defect but the fractional volume of the sample occupied by
these defects.   For this purpose we let

$$ f_p = \frac{dG}{dr} \frac{V_n}{V} \ (\text{dynes}/\text{cm}^3) \tag{36} $$

where $V_n/V$ is the fraction of the volume occupied by normal inclusions.
The current density is then $j = cf_p/B$ $(\text{statamperes}/\text{cm}^2)$   This current
density is shown in Figure 10 in amperes/$\text{cm}^2$ without correction for the
term $V_n/V$.   If in a particular sample 0.1% of the sample were occupied
by normal inclusions, the current density in Figure 10 would be multi-
plied by $10^{-3}$   This current density is compared with the functional
form $(1 - H/H_{c2})/(H/H_{c2})^{\frac{1}{2}}$ which has been compared with experiment and
discussed elsewhere [8,23,24]

Voids of the type just discussed are rare in comparison with the
numerous other types of defects found in metals, with the exception of
sintered materials which can contain a large number of voids   It is
of interest to determine the effect on the current density of small in-
clusions that have a $\varkappa$ value different than that of the host lattice
In this case, the volume pinning force is

24
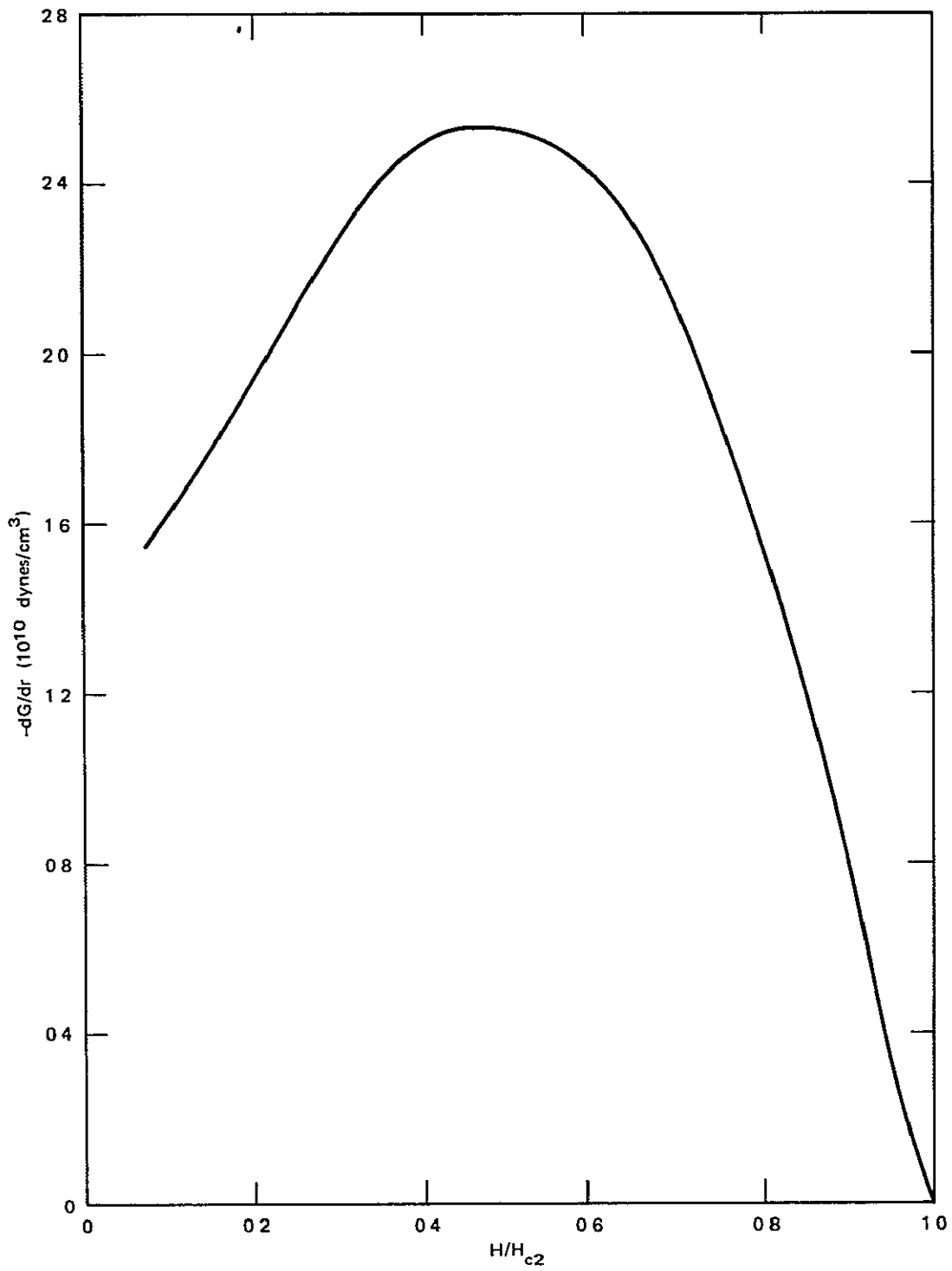
FIGURE 9    MAXIMUM PINNING FORCE PER UNIT VOLUME OF SMALL NORMAL
            INCLUSIONS INSIDE A FLUXOID FOR THE CASE $\kappa$ = 5,
            $H_c$ = 2 x $10^3$ Oe  AND $\lambda$ = 7 5 x $10^{-6}$ cm

25
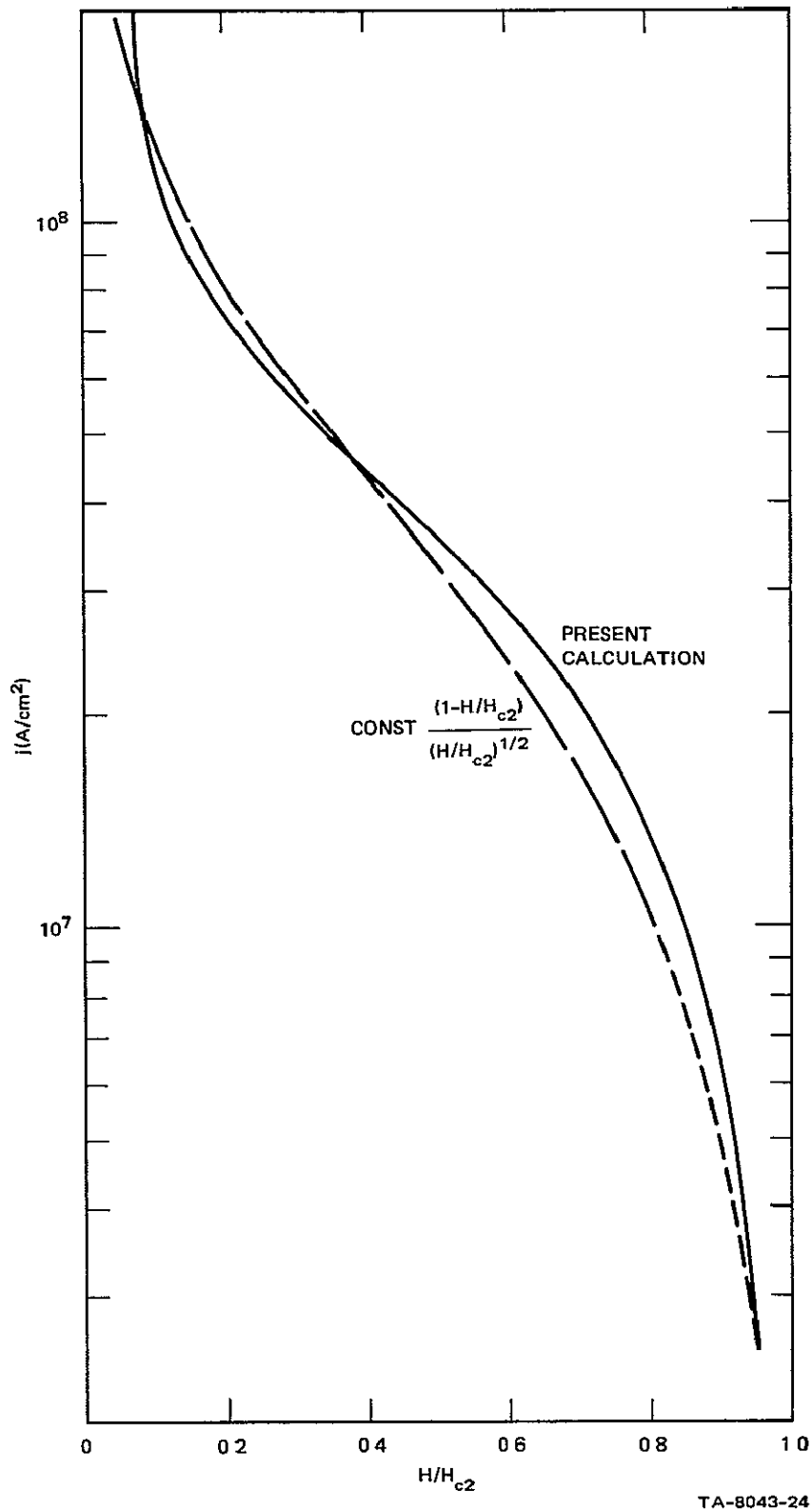
FIGURE 10    CURRENT DENSITY CAUSED BY SMALL DISPERSED
NORMAL INCLUSIONS IN A SUPERCONDUCTOR, $\kappa$ = 5
Multiply values shown by volume fraction of sample contained
in normal inclusions

26

$$F_p = \frac{\partial^2 G}{\partial \varkappa \partial r} \frac{V_\varkappa}{V} \Delta \varkappa \qquad (37)$$

where $V_\varkappa/V$ is the relative volume of the material having a different value of $\varkappa$

This derivative was evaluated numerically but met with difficulties at low fields that have not been resolved at present    The maximum value of the pinning force in the fluxoid is shown in Figure 11    The shape of this curve differs radically from those shown earlier    A pronounced peak occurs at high fields    It was found that although $\partial G/\partial r$ decreased at high fields, the difference between values calculated for slightly differing $\varkappa$ values (a 0.5% change was used in obtaining the derivatives)



TA-8043-27

FIGURE 11    VOLUME FORCE CAUSED BY SMALL DISPERSED INCLUSIONS HAVING VALUES OF $\kappa$ DIFFERING FROM THE HOST MATERIAL   Multiply values shown by the volume fraction of the sample having the different value of $\kappa$

27

increased with field   It is assumed that since $\partial G/\partial r$ vanishes at $H_{c2}$ for the bulk of the sample, the pinning force will vanish at this field.

It is not possible to calculate values at higher fields without resorting to double precision computations which time did not permit These calculations were considerably more difficult to handle than those previously discussed since the absolute energy must be known with great precision.   The Bessel functions were calculated to an accuracy of only one part in $10^{10}$   At low fields, the arguments of the functions become large and oscillations occurred about the asymptotic value, limiting the accuracy to as little as one part in $10^8$   At this time we are unable to state the cause of scatter in the results at low fields.   It may be caused by the loss of precision, or by insufficient minimization of the energy with respect to $N$ and $\epsilon$.

The curve drawn in Figure 11 is a reasonable approximation to the calculated points and has been used to determine the average critical current density shown in Figure 12.   This curve obviously depicts the well-known "peak effect" often observed in type-II superconductors.   To obtain the actual critical current density in a sample, the current density shown must be multiplied by the volume fraction of the sample occupied by the inclusions having different values of $\varkappa$ and by $\Delta\varkappa$

In the following section, we will show that a whole spectrum of values of $\varkappa$ can occur in a sample, even in samples that are well annealed Consequently, in most samples there will not be one value of $\Delta\varkappa$ but several, and the current density will have contributions from more than one curve such as that shown   Further, rather than having a sharply defined change in $\varkappa$ there is a distribution in $\varkappa$ about a central $\Delta\varkappa$. This will cause a smearing of the curve shown for most samples.   The peak effect has been introduced into at least one niobium-zirconium sample by radiation damage.[14]   This type of experiment introduces rather
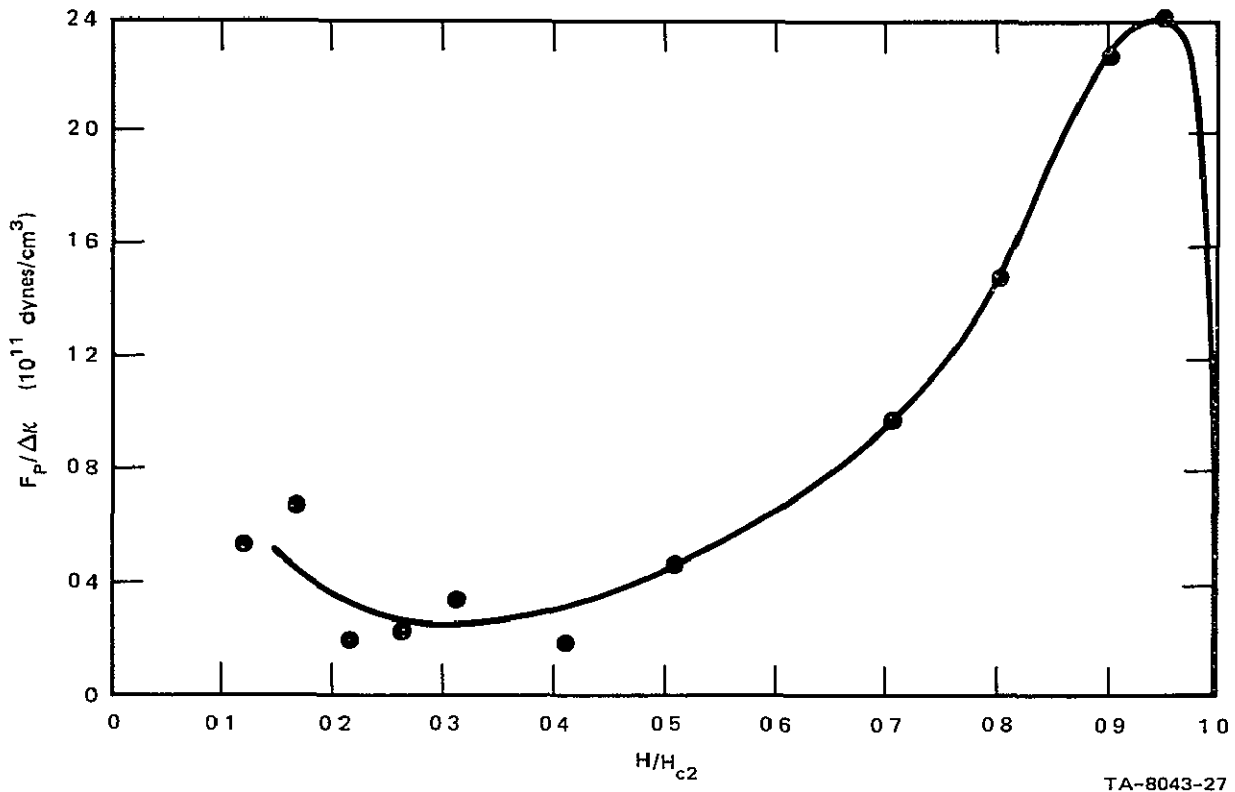
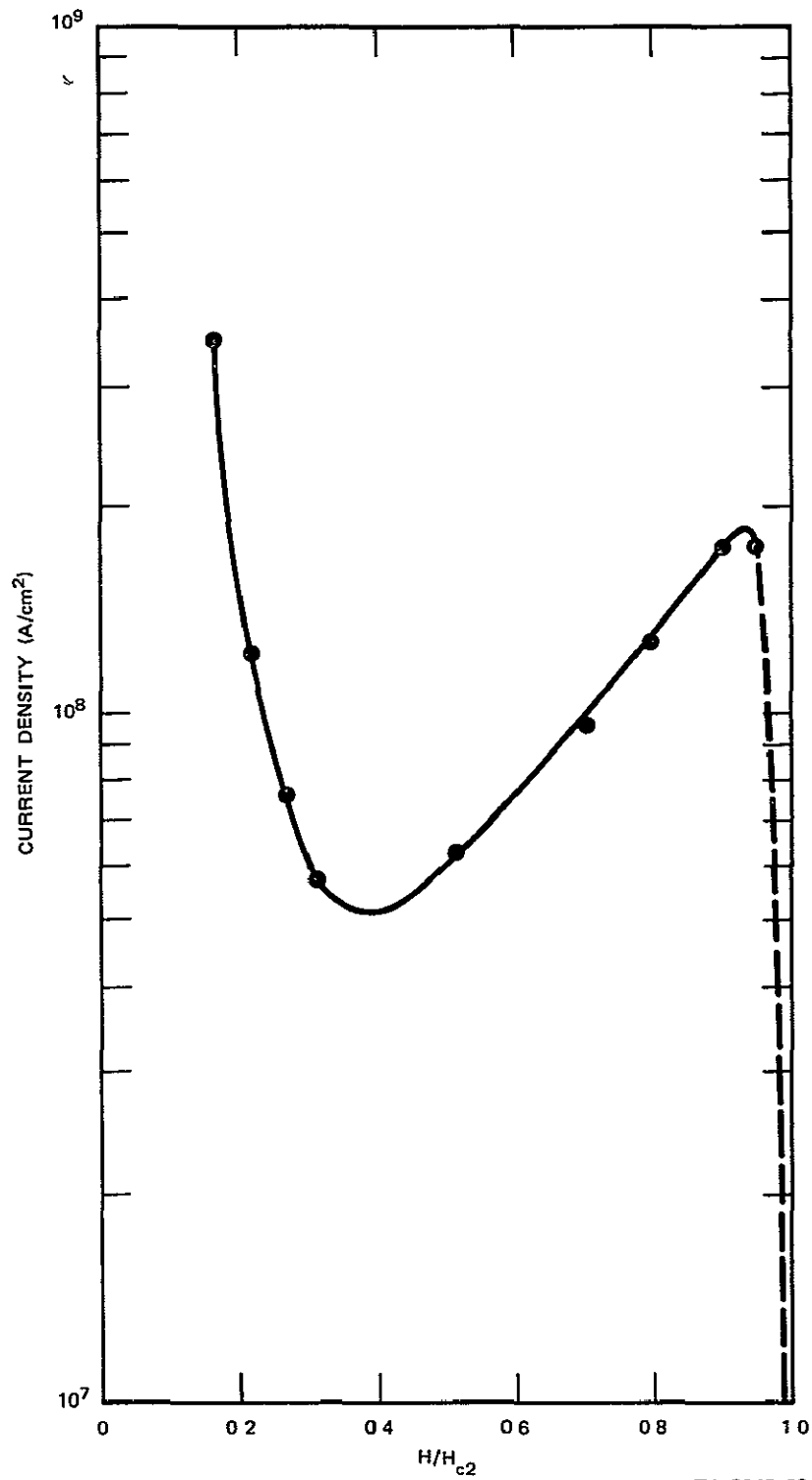FIGURE 12    CURRENT DENSITY CAUSED BY SMALL DISPERSED
INCLUSIONS HAVING VALUES OF $\kappa$ DIFFERING
FROM THE HOST MATERIAL    Multiply values shown
by the volume fraction of the sample having the different
value of $\kappa$ and by $\Delta\kappa$

29

well-defined clusters of displaced atoms that should yield a fairly sharply defined $\Delta\varkappa$  It should be noted, however, that other samples of different materials did not exhibit this effect

The volume fraction of the sample occupied by these defects must be small for this calculation to be valid  For this reason, the critical current density contributed by this phenomenon will be relatively small and the effect will be noticed only at high fields where the critical current density caused by the other mechanisms discussed is small

The force exerted on the pinning site by the fluxoid is not always of the same sign, but can be attractive or replusive at different positions For a positive $\Delta\varkappa$, the largest force is always attractive near the center of the fluxoid, but can be repulsive near the outer radius at low fields (this is thought to be true even though the absolute magnitude is in doubt for the reasons discussed earlier).  At high fields, the force is attractive all the way to the outer radius.  The form of the force at $B/H_{c2} = 0.3$ is shown in Figure 13  Obviously, if there is more than one pinning site inside the fluxoid there is a high probability that the forces exerted on the two sites will tend to oppose each other and an average force is needed  This behavior persisted in the present case to a field of about 0.6 $H_{c2}$.  At higher fields, the force was attractive all the way to the outer radius of the fluxoid.

Conclusion

The model developed is sufficiently accurate to permit detailed calculations of features of fluxoids in type-II superconductors which could not be calculated previously.  The model can be used to determine all the usual physical properties of fluxoids such as energy, energy distribution, magnetic induction, induction distribution, current density distribution, magnetic field, and magnetization
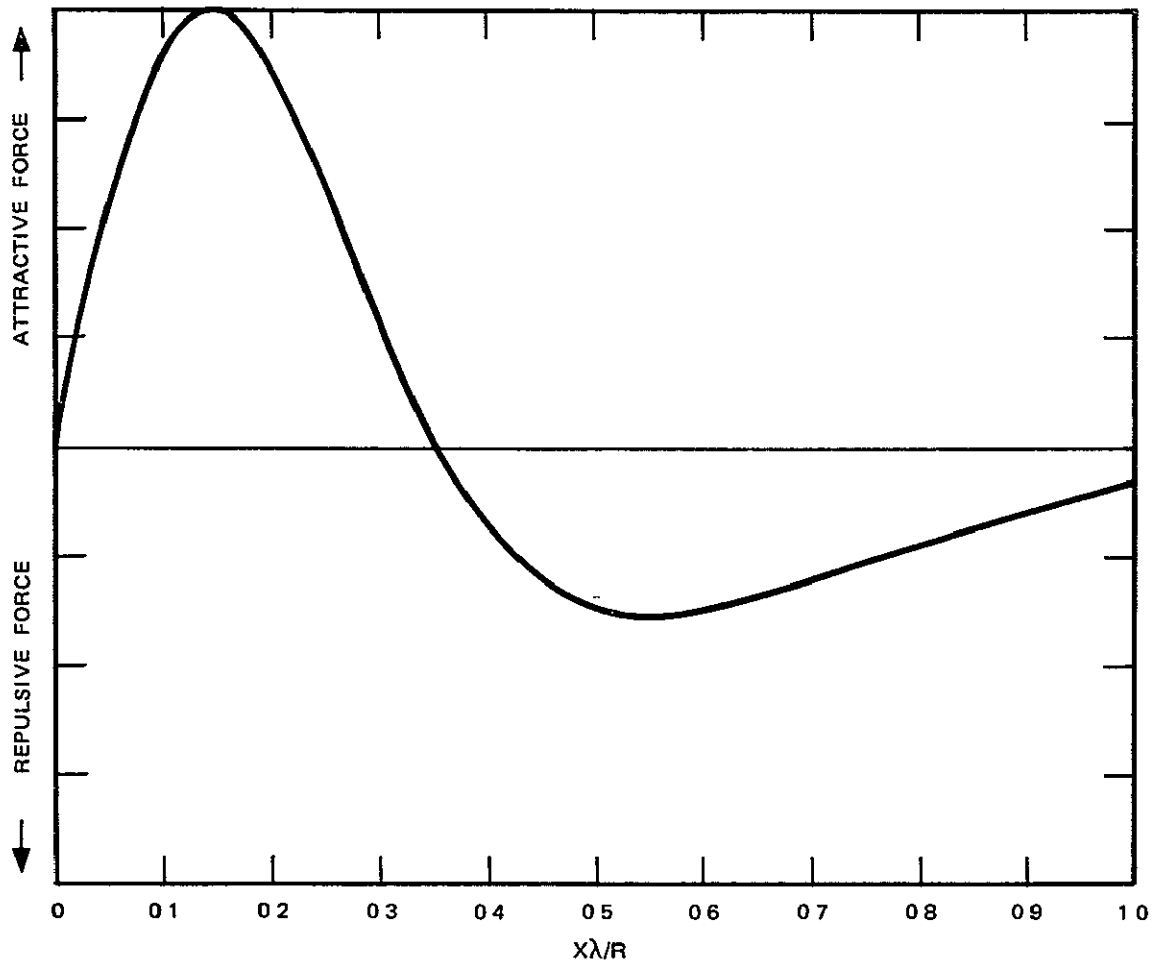
TA-8043-26

FIGURE 13    FORCE EXERTED ON A FLUXOID BY A SMALL INCLUSION HAVING A VALUE OF $\kappa$ DIFFERENT THAN THAT OF THE HOST MATERIAL FOR THE CASE $\kappa$ = 5 AND $B/H_{c2}$ = 0 3 (ARBITRARY SCALE)    At high fields the attractive force extends to the outer radius of the fluxoid

This model was used to calculate the forces exerted on a fluxoid by several simple types of pinning centers   (1) large defects with gradients in $\varkappa$, (2) extremely small voids, and (3) small inclusions with values of $\varkappa$ different from that of the host lattice.  These forces were related to the current densities that can be sustained by materials containing these defects.  The resulting jc versus H curves are similar in form and magnitude to the curves generally observed experimentally   The third type of pinning center indicated above had unusual properties, yielding a $J_c$ versus H curve with a peak in j near $H_{c2}$   Further, it was found that although the strongest pinning force was always attractive for a positive $\Delta\varkappa$ in the inclusions, inclusions near the outer radius of the fluxoid can cause a repulsive force.

# SPECIFIC HEAT CAPACITY

## Theoretical Analysis

The specific heat of a homogeneous annealed sample can be characterized by the material parameters $\varkappa$ and $T_o \equiv T_c (H = 0)$

When the material is strained, we observe that the specific heat discontinuity in zero field is smeared out  This means that the strained material must be characterized by a distribution in $T_o$ Further, the strained material in nonzero fields displays an even larger temperature smearing of the specific heat than in zero field This means that in addition to the $T_o$ distribution there is also a distribution in $\varkappa$  We have developed a formalism that describes and permits solving for such $\varkappa$ and $T_o$ distributions  It serves also as a posteriori justification of the assertions

The essential point in this theory is that the temperature variation of the specific heat near the transition is extremely sensitive to variations in material parameters  Away from the transition, the specific heat is particularly insensitive and, indeed, not predictable from theory with enough accuracy to determine material parameter distributions

To obtain a useful specific heat expression which displays the discontinuity, the normal electronic specific heat, which at low temperature equals $\gamma_e T$, is subtracted from the total specific heat C. This function for particular values of $T_o$, $H_o \equiv H_c(T = 0)$, $\varkappa$ is

$$f(T, H, T_o, H_o, \varkappa) = \frac{C - \gamma_e T}{T} \equiv f_1(T, H, T_o, H_o, \varkappa) \, \mathcal{H}\left(T_c(h) - T\right) \quad (38)$$

where C is the specific heat    The Heaviside unit function $\mathcal{H}(T_c(H) - T)$
expresses the discontinuity    The functional form away from the discon-
tinuity is contained in $f_1$    One of the better expressions for $f_1$ is
that of Van Vijfeijken[25]

$$f_1(T, H, T_0, H_0, \varkappa) = \frac{\varkappa^2}{\varkappa^2 - \text{Log } \varkappa} \left[ 3\left(\frac{T}{T_0}\right)^2 + \frac{H}{\sqrt{2}\varkappa H_0} - 1 \right] \tag{39}$$

The measured specific heat in a strained material at fixed H would
include contributions from all values of $T_0$ and $\varkappa$ present in the material,

$$\bar{f}(T, H) = \int dT_0 d\varkappa P_{T_0}(T_0) P_\varkappa(\varkappa) f_1(T, H, T_0, H_0, \varkappa) \, \mathcal{H}(T_0(H) - T). \tag{40}$$

The experimental data imply that distributions in two parameters
are required    If the microscopic basis for the $T_0$ and $\varkappa$ distributions
were understood, it might result that these distributions were related

The sensitivity of the discontinuity to the material parameters
is best identified in the derivative $d\bar{f}/dT$, which would be infinite for
a homogeneous, annealed material

$$\frac{d\bar{f}}{dT} = \int dT_0 d\varkappa \, P_{T_0}(T_0) \, P_\varkappa(\varkappa) \left[ \frac{df_1}{dT} \, \mathcal{H}(T_c - T) - f_1 \delta(T_c - T) \right] \tag{41}$$

In the region where $\overline{df/dT}$ is large, only the second term makes a non-
negligible contribution,

$$\frac{d\bar{f}}{dT} \approx - \int dT_0 d\varkappa \, P_{T_0}(T_0) \, P_\varkappa(\varkappa) \, f_1 \, \delta(T_c - T) \tag{42}$$

Further reduction of equation (42) requires a functional form for

$T_c(H, T_o, \varkappa)$    For most materials, in the vicinity of $T_o$

$$H_{c2}(T) = \sqrt{2}\varkappa\, H_o \left( 1 - (\frac{T}{T_o})^2 \right) \tag{43}$$

At the transition $H = H_{c2}$ equation (43) inverts

$$T_c(H, T_o, \varkappa) = T_o \left( 1 - \frac{H}{\sqrt{2}\varkappa\, H_o} \right)^{\frac{1}{2}}. \tag{44}$$

This form applies to a variety of type-II superconductors    Use of more precise and more complicated forms for equations, (43) and (44) has only a minor effect on the results below

Further reduction of equation (42) must be performed before data can be analyzed    In zero field, the argument of the $\delta$ function has only a $T_o$ dependence    The temperature dependence becomes

$$\left. \frac{d\bar{f}}{dT} \right|_{H = 0} \approx P_{T_o}(T) \int d\varkappa P_{\varkappa}(\varkappa) f_1(T, \varkappa) \tag{45}$$

In nearly every form conceivable for $f_1$, the variable $T_o$ would occur as $T/T_o$.  Therefore equation (45) is $P_{T_o}(T)$ multiplied by a constant that is later absorbed in the normalization.  Since we want $P_{T_o}(T)$ normalized such that its intergal is unity,

$$\int dT_o\, P_{T_o}(T_o) = 1 \tag{46}$$

equation (45) is an algorithm for determining $P_{T_o}(T)$ directly from the experimental data

When the magnetic field is not zero, a modification of the above approach must be used to determine the $\varkappa$ distribution   Note that in equation (44) for $T_c$, $\varkappa$ appears only in the form $\varkappa\sqrt{2}H_0 \equiv H_{c_2}$.   This implies that the observable is really $H_{c_2}$, hence our analysis of the $\varkappa$ distributions will be in the form of $H_{c_2}$ distributions   Equation (42) is changed to

$$\frac{d\overline{f}}{dT} \approx -\int dT_0 dH_{c_2} \; P_{T_0}(T_0) \; P_{H_{c_2}}(H_{c_2}) \; f_1 \; \delta(T_c - T) \tag{42$'$}$$

and equation (44) becomes

$$T_c(H, \; T_0, \; H_{c_2}) = T_0\left(1 - \frac{H}{H_{c_2}}\right)^{\frac{1}{2}} \tag{44$'$}$$

First examination of equation (42$'$) would suggest that we have a hopeless unfolding problem, because elimination of the one $\delta$ function will still result in an integral over $P_{T_0}$ and $P_{H_{c_2}}$   Thus, we would have at best, a Fredholm integral equation of the first kind for $P_{H_{c_2}}$

This is not the case, however, for elimination of the delta function in equation (42$'$) gives us an integral over two distributions, each of which is fairly narrow or peaked   To examine their relative contributions to the derivative of the specific heat given by equation (42$'$), we can take the derivative with respect to temperature of the argument of the function as given by equation (44$'$)   The result is

$$\frac{\Delta T}{T} = \frac{\Delta T_0}{T_0} + \frac{1}{2} \frac{H/H_{c_2}}{1 - H/H_{c_2}} \frac{\Delta H_{c_2}}{H_{c_2}} \tag{47}$$

The important point is that the contribution to the width of the tran-
sition consists of two parts, one due to the distribution in $T_0$ and one
due to the distribution in $H_{c_2}$   The latter distribution has its width
multiplied by a factor that is quite large at high fields   For example,
at field values near the largest value for which measurements were taken,
2,700 gauss, the contribution of the $T_0$ distribution to the width of the
specific heat transition was less than 5% of the contribution  due to
the $H_{c_2}$ distribution.  This means that in the evaluation of equation
$(42')$ (for the purpose of analysis of the data in high fields), it is
quite satisfactory to treat the $T_0$ distribution as a delta function,
$P_{T_0} = \delta(T_0 - \overline{T}_0)$   We then obtain the following equation for the $H_{c_2}$ dis-
tribution

$$\frac{d\overline{f}}{dT^2} \approx \frac{H \, P_{H_{c_2}}\left(H_{c_2}\right)^*}{\overline{T}_0^{\,2}\left(1 - \left(\frac{T}{T_0}\right)^2\right)} \; f_1(T,\; H,\; \overline{T}_0,\; H_{c_2})^* \qquad (48)$$

where

$$H_{c_2}^{\;*} = \frac{H}{1 - \left(\dfrac{T}{T_0}\right)^2} \qquad (49)$$

Equation (48) and (49), plus the normalization condition $\int P_{H_{c_2}} dH_{c_2} = 1$,

provide a complete algorithm for analyzing specific heat data for $H_{c_2}$

distributions.  Because of the considerations implied by equation (47),
it is worth while to do such an analysis only at large values of fields

37

## Specific Heat Measurements, Data, and Analysis

The heat capacity of high purity niobium samples was measured using the apparatus shown in Figure 14   This device uses an ac calorimetry technique developed by Sullivan and Seidel[26]

In the apparatus shown in Figure 14, a laser beam which is chopped at a known frequency, $\omega$, is used to heat a sample   The temperature of the sample rises above that of the copper reference block by an amount, $\Delta T$, determined by the equation at the bottom of the diagram.  The equation states that this temperature rise consists of two parts   (1) a dc temperature rise given by $Q_o/k$ and, (2) an ac temperature rise proportional to $1/C$.  This temperature change, $\Delta T$, is measured by using a gold-iron versus copper thermocouple.  The thermocouple is mounted on the sample and coupled to a copper reference block whose temperature is measured using a dc thermocouple connected to a Keithley-type 147 nanovolt-meter.  The actual increase in dc temperature above the temperature of the block is determined from the thermocouple by using the nanovoltmeter  An ac signal is produced in the thermocouples by the temperature rise and is amplified through a low temperature transformer   The signal is measured by a PAR HR-8 lock-in amplifier tuned to the same frequency, $\omega$, as the chopped laser beam

It should be noted that there are some correction terms in the ac temperature rise that do not make it strictly proportional to $1/C$.  By judicious choice of $\omega$, $\tau_1$ (relaxation time to block determined by the thermal conductivity of the thermocouple wires), and $\tau_2$ (thermal relaxation time across the sample itself), the correction terms can usually be made less than 1%.  Thus by properly choosing $\omega$, $\tau_1$, and $\tau_2$, the ac temperature rise can be measured accurately   However, to make an absolute measurement of the heat capacity, $\dot{Q}_o$ must be known accurately

An effective measure of the $Q_o$ is made by using a standard sample of known heat capacity (usually copper) in one of the two chambers shown in Figure 14   The laser light, and its associated $\dot{Q}_o$, produce an ac signal   This signal is assumed to be inversely proportional to the heat capacity of the known sample   By measuring the ratio of the two ac signals with the same $\dot{Q}_o$, and at the same temperature, an absolute measure of the heat capacity of the unknown sample can be determined
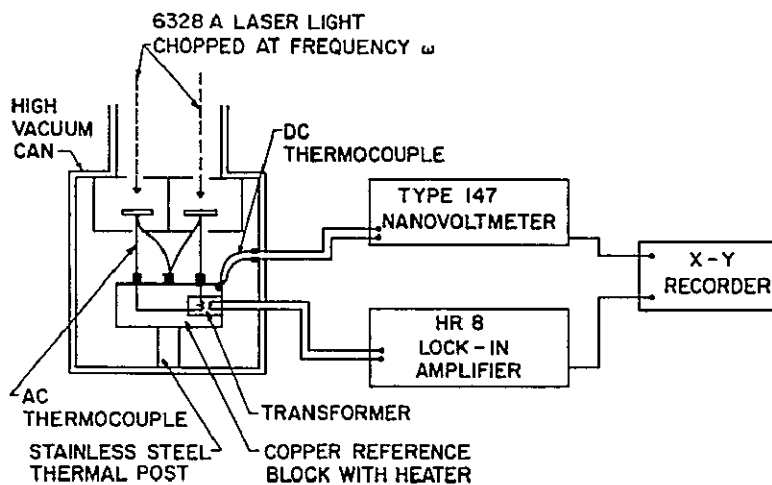


$$\Delta T = \frac{Q_o}{K} + \frac{Q_o}{\omega C} \left[ 1 + (\omega \tau_1)^{-2} + (\omega \tau_2)^2 \right]^{-\frac{1}{2}} \cos(\omega t + \alpha)$$

TA-8043-38

FIGURE 14   SPECIFIC HEAT APPARATUS

As primary advantages, this technique has the ability to measure relative changes in heat capacity as a function of temperature with a precision of about 0 1%, and the ability to make continuous measurements of heat capacity as the temperature is varied thereby increasing the speed of the data-taking process   Furthermore, since the mass of the additional apparatus required to sense the temperature and heat the sample has been minimized, an absolute measurement of the heat capacity of samples whose weights are approximately 150 mg or less, can be made with an accuracy of approximately 3%

The temperature resolution is approximately 1 mK while the absolute accuracy is approximately 20 mK  The accuracy of the magnetic field measurement is approximately 1%, which implies a 28 gauss probable error at the highest field measured of 2,745 gauss

The niobium specific heat capacity data is shown in Figures 15, 16, 17, and 18 as measured for four different field ranges near zero, 500, 1,300, and 2,700 gauss  Four different samples were measured.  The first was an annealed sample.  The second had a strain of 0.07.  The third had a strain of 0.20, and the fourth had a strain of 0.75.  The strains were introduced by rolling  The measurements in zero field show a systematic increase of transition temperature with strain, and a systematic increase of width of the specific heat transition with strain  The results near 500 gauss resemble the results of zero field with the exception of
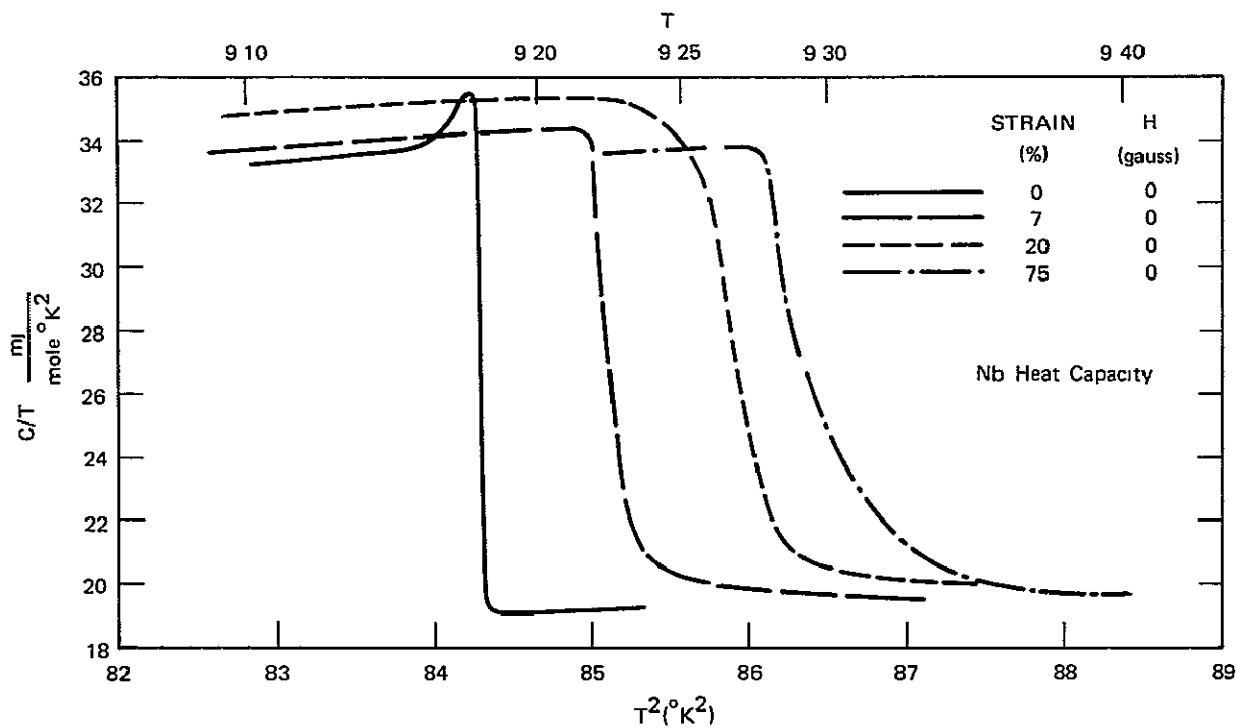


FIGURE 15  SPECIFIC HEAT OF STRAINED AND UNSTRAINED NIOBIUM SAMPLES
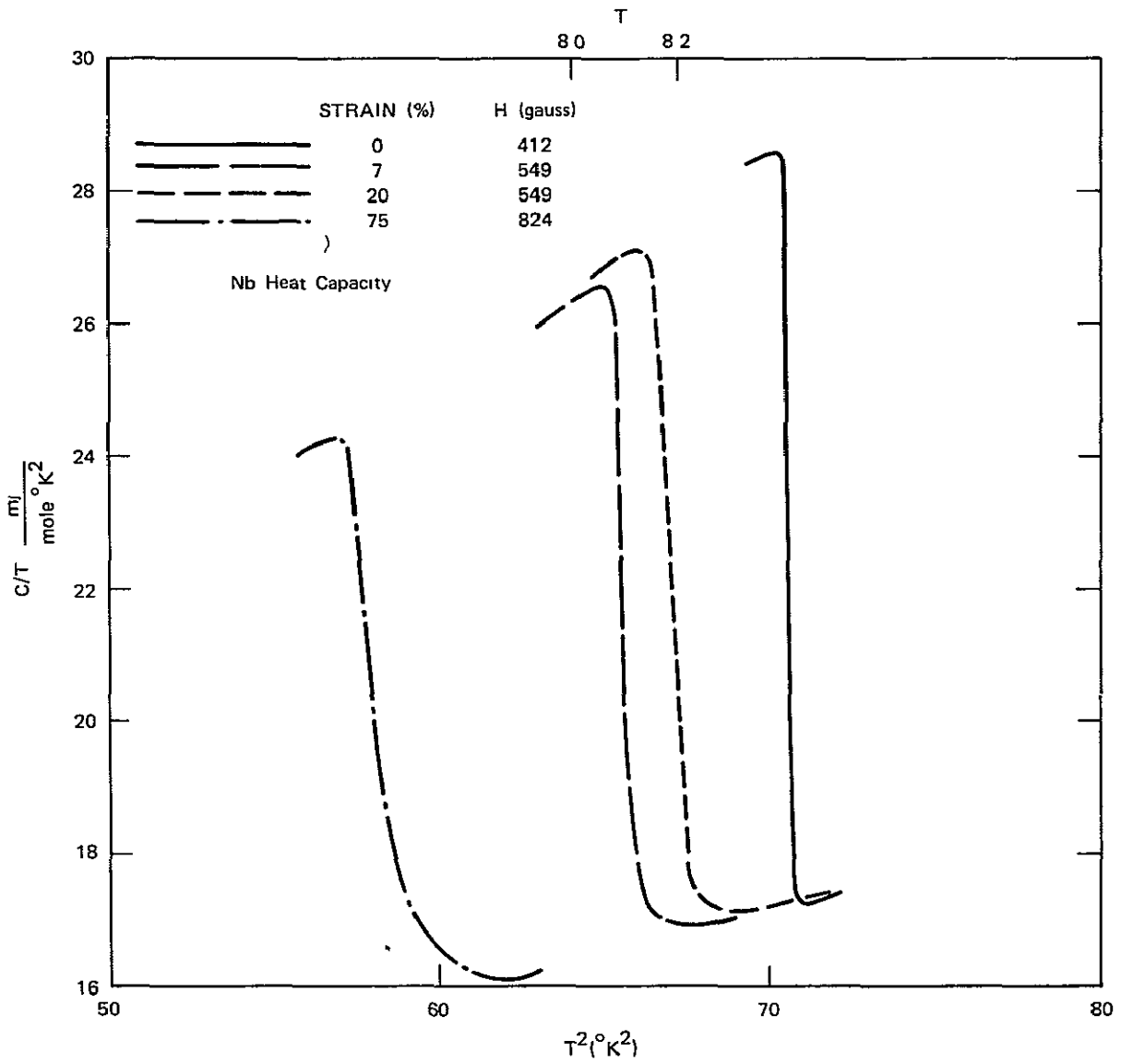
FIGURE 16 SPECIFIC HEAT OF STRAINED AND UNSTRAINED NIOBIUM SAMPLES AT VARIOUS APPLIED FIELDS

TA-8043-16

41

20

19

Nb Heat Capacity

$C/T$ $\dfrac{\text{mj}}{\text{mole }^\circ\text{K}^2}$

18

17

16

15

| STRAIN (%) | H (gauss) |
|---|---|
| 0 | 1373 |
| 7 | 1373 |
| 20 | 1373 |
| 75 | 1510 |

14

13

37   38   39   40   41   42   43   44   45   46   47
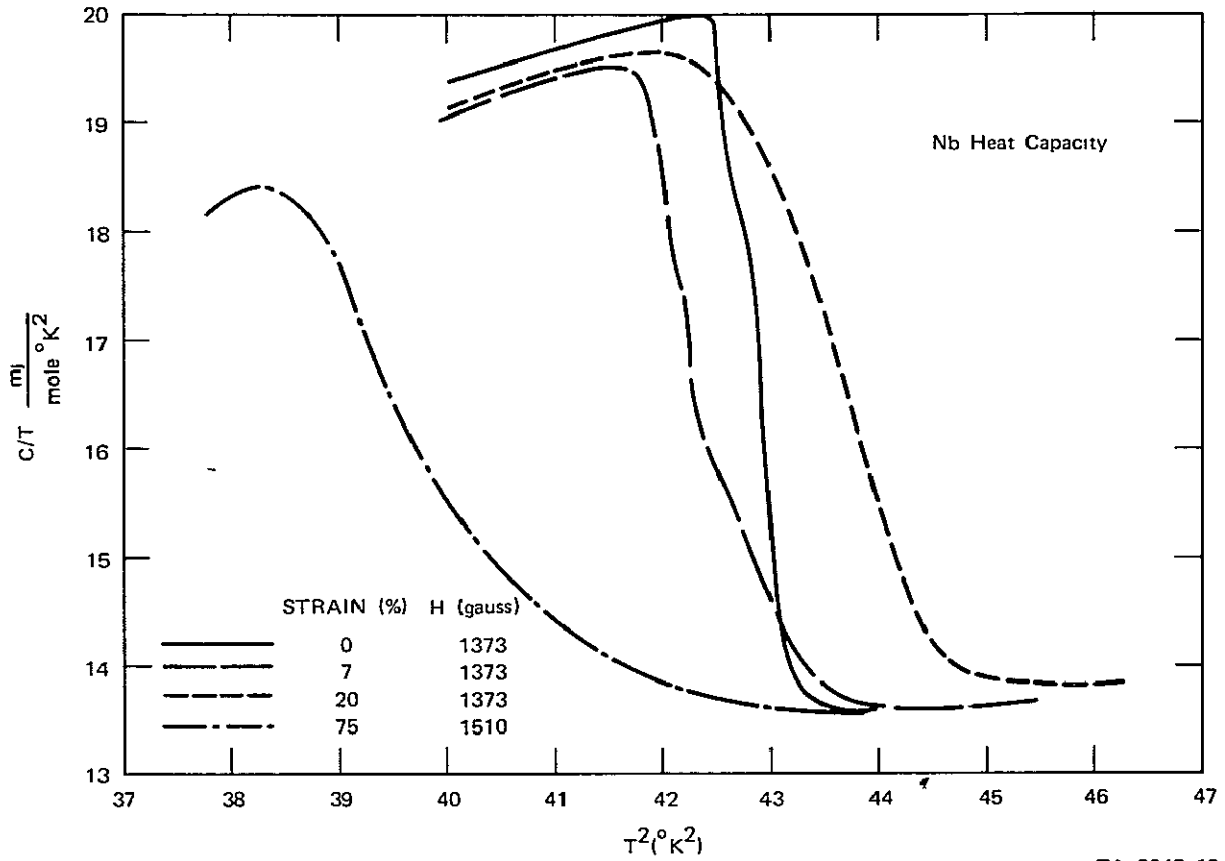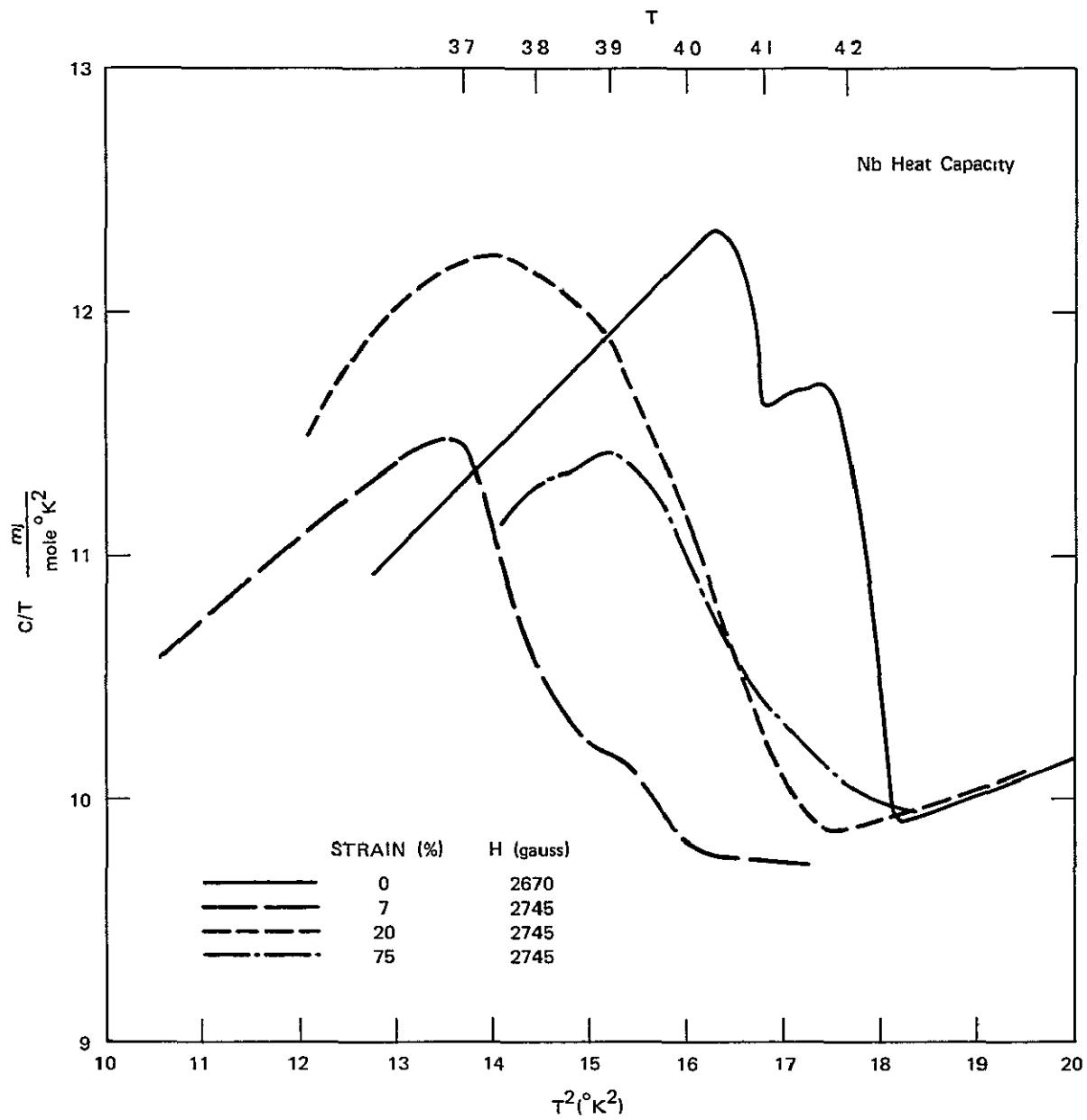
$T^2(^\circ K^2)$

TA-8043-19

FIGURE 17  SPECIFIC HEAT OF STRAINED AND UNSTRAINED NIOBIUM SAMPLES AT VARIOUS APPLIED FIELDS

FIGURE 18  SPECIFIC HEAT OF STRAINED AND UNSTRAINED NIOBIUM SAMPLES
AT VARIOUS APPLIED FIELDS

TA-8043-18

43

the shifting of the relative positions of the curves due to the varia-
tions of magnetic field strength  The change of character that is noted
in the results at 1,300 and 2,700 gauss is due to the shift of the tran-
sition width from a transition that is dominated by the $T_o$ distribution
to one dominated by the $\varkappa$ or $H_{c2}$ distribution as described in equation (47)


## $T_o$ Distribution

Taking the derivative of the specific heat with respect to the
temperature from the data shown in Figure 15 for zero fields yields the
$T_o$ distribution as given in equation (45)

The $T_o$ distribution of the annealed sample is a delta function or
a gaussian distribution with a standard deviation of less than 0 5 mK
Figure 19 shows the $T_0$ distribution for a strain of 0 07.  This distribu
tion is fit reasonably well by assuming a gaussian distribution with
$T_0 = 9.225$ K and a standard deviation of 4 mK  When the strain reaches 0.20,
the distribution is broadened as shown in Figure 20.  This distribution is
still sufficiently well fit by a gaussian distribution with $\overline{T}_0 = 9\ 268$ K
and a standard deviation of 11 mK  Note that there is a high temperature
tail that extends several standard deviations above $\overline{T}_o$.  When the strain
is as large as 0 75 as shown in Figure 21, we found that the distribution
of $T_o$ was broadened considerably and not even close to a gaussian dis-
tribution in shape  The distribution extends many times as far above
the mode of the transition temperature, $\overline{T}_o = 9\ 285$, as it does below $\overline{T}_o$
The distribution to higher temperatures appears more exponential-like
than gaussian  The behavior of the modes, $\overline{T}_o$, versus strain as shown in
Figure 22, indicates that for small strain there is a rapid increase in
$T_o$ with strain, and for large strain there is an asymptotic approach to
a maximum value at $\epsilon = 1.0$  It is useful also to show how the width of
the transition changes with strain in Figure 23  The width is defined

TA-8043-29
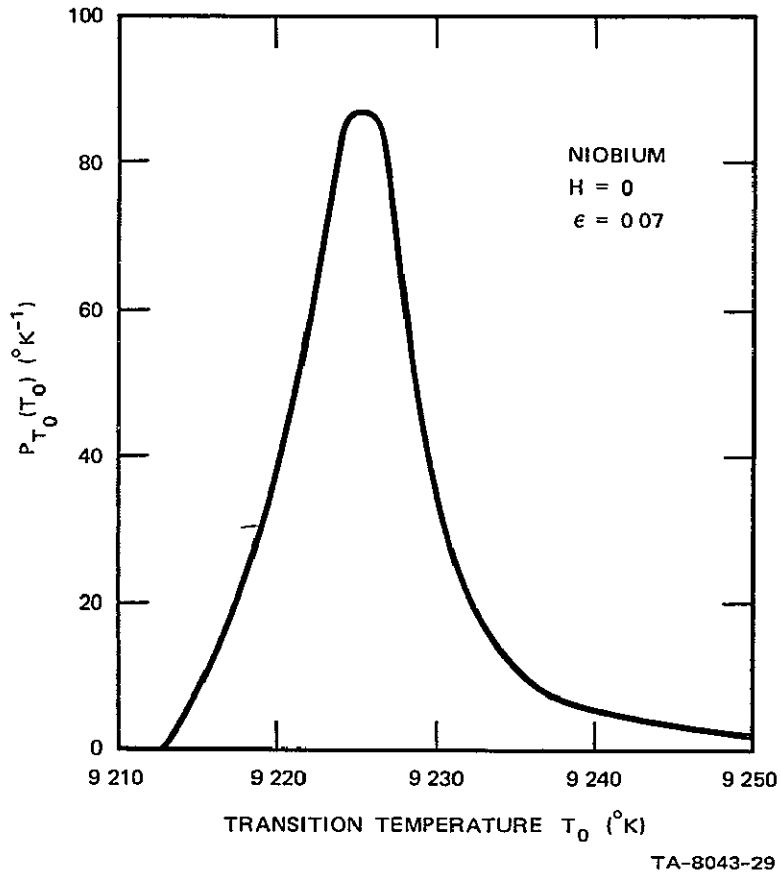
FIGURE 19    DISTRIBUTION IN $T_0$ FOR A NIOBIUM SAMPLE
OBTAINED FROM SPECIFIC HEAT CAPACITY
MEASUREMENTS IN ZERO FIELD    The strain
was 0 07

45

TA-8043-30

FIGURE 20    DISTRIBUTION IN $T_0$ FOR A NIOBIUM SAMPLE OBTAINED FROM SPECIFIC
HEAT CAPACITY MEASUREMENTS IN ZERO FIELD    The strain was 0 20
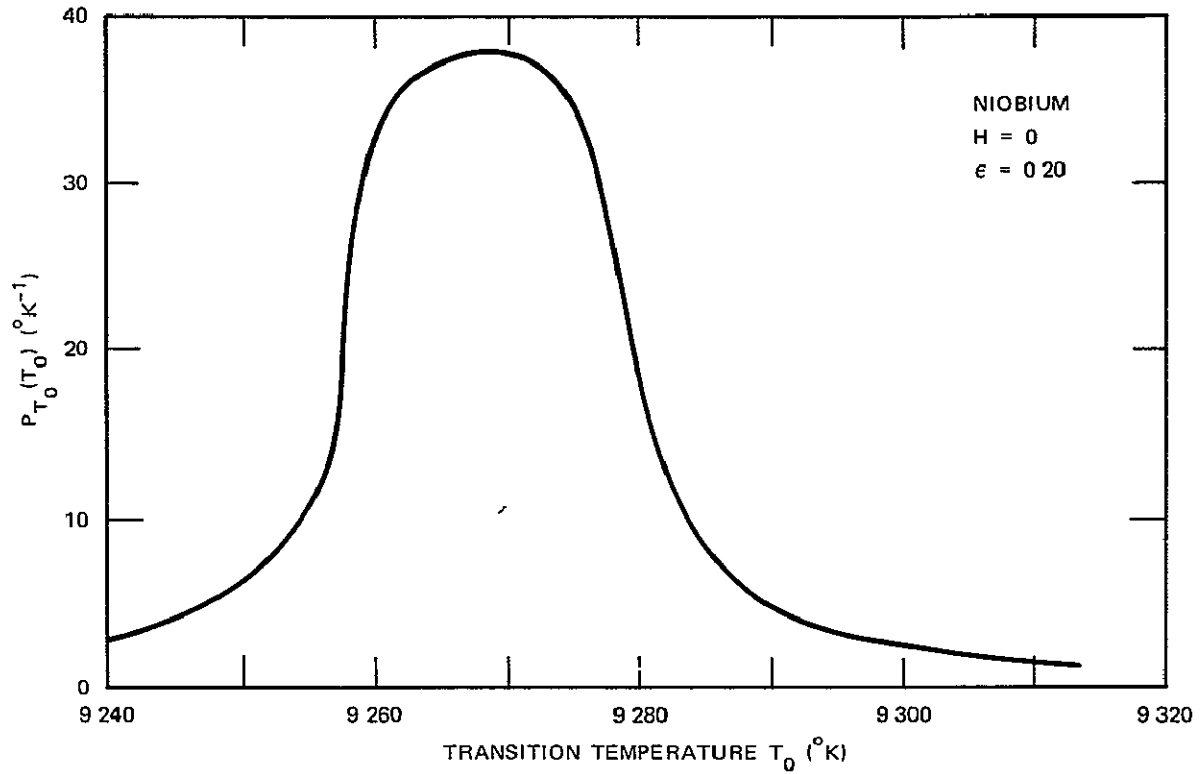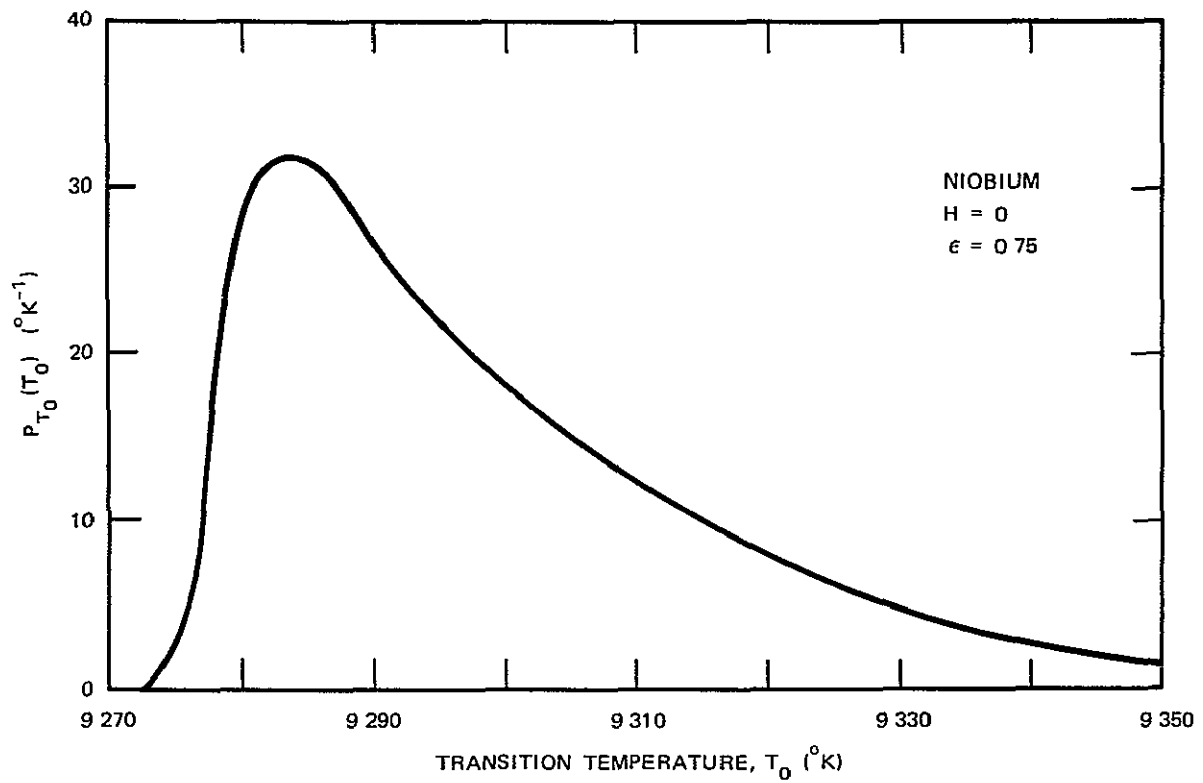
NIOBIUM
H = 0
$\epsilon$ = 0 75

TA-8043-31

FIGURE 21   DISTRIBUTION IN $T_0$ OBTAINED FROM SPECIFIC HEAT CAPACITY
MEASUREMENTS IN ZERO FIELD   The strain was 0 75

47

TA-8043-32
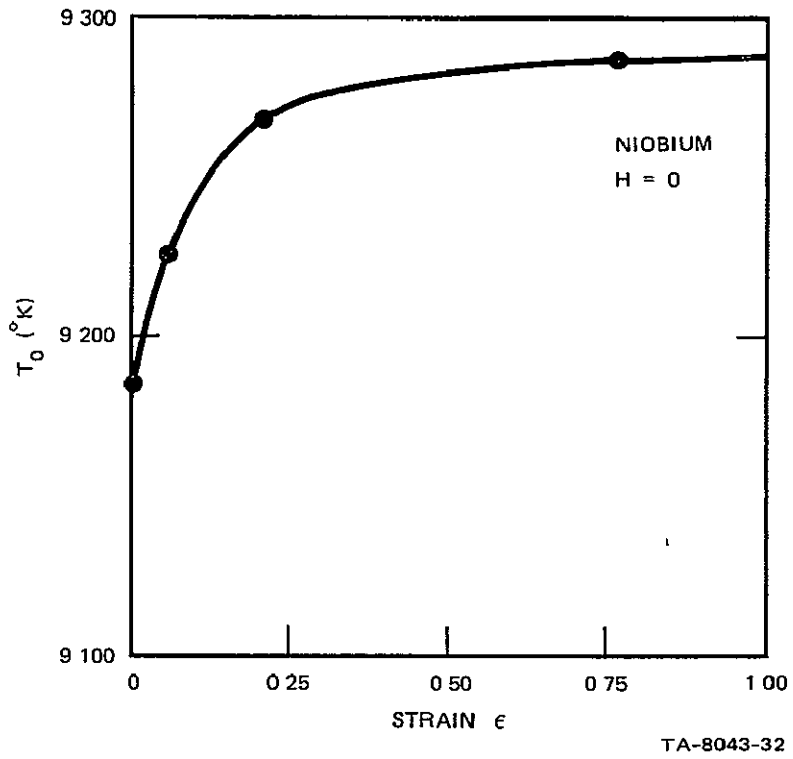
FIGURE 22    CHANGE OF MODE TRANSITION TEMPERATURE
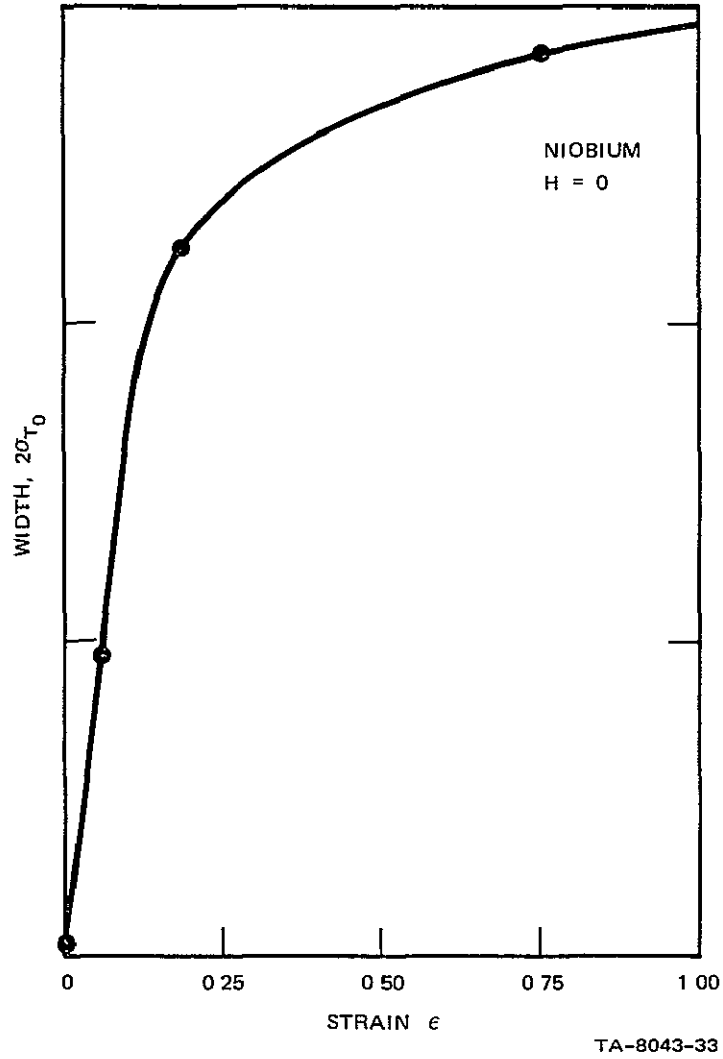WITH STRAIN IN NIOBIUM

48

FIGURE 23    CHANGE OF WIDTH OF THE $T_0$
DISTRIBUTION WITH STRAIN IN
NIOBIUM

49

as the half width at a relative height of 0 135 of maximum height   For
a gaussian distribution such a definition of width would yield twice the
standard deviation   The width increases rapidly with strain for small
strain, but shows a much lower derivative for large strain

## $H_{c2}$ or $\varkappa$ Distributions

Analysis of the high field specific heat measurements near 2,700
gauss, according to the algorithm of equations $(48)$ and $(49)$, yield the
$H_{c2}$ or $\varkappa$ distributions shown in Figures 24, 25, 26, and 27   Figure 24
shows the $\varkappa$ distribution for zero strain   The results were surprising
because they indicate two narrow, clearly separated distributions in $\varkappa$
The relative separation is approximately 2%   From earlier work with a
less quantitative model,[27] we had expected such a behavior to be more
likely in highly strained samples in which there is a well-defined cell
wall structure   The lower peak with $\overline{H}_{c2} = 3,333$ has approximately 33%
of the area of the entire $H_{c2}$ distribution.   The upper peak occurs at
$\overline{H}_{c2} = 3,395$   The $\varkappa$ scale uses $H_o = 1,993$ gauss for niobium as obtained
by Finnemore, Stromberg, and Swenson[28]

In the sample with 0 07 strain shown in Figure 25, the same basic
structure persists except that each of the peaks have been broadened
and the relative magnitude has changed   For 0 07 strain $\overline{H}_{c2} = 3,293$
and 3,358   We do not regard the shifts of peak position as significant
because a 37-gauss shift, which is only slightly more than the probable
error for the field measurements, would cause the two structures to be
in agreement

The sample which was strained to 0.20 and is shown in Figure 26,
demonstrates that the distributions have been broadened further into
two plateaus and the structure at the lower value of $\varkappa$ was nearly de-
pleted at the expense of the peak at the higher value of $\varkappa$   Figure 27
for a strain of 0 75 shows a behavior in the $H_{c2}$ or $\varkappa$ distribution that

50
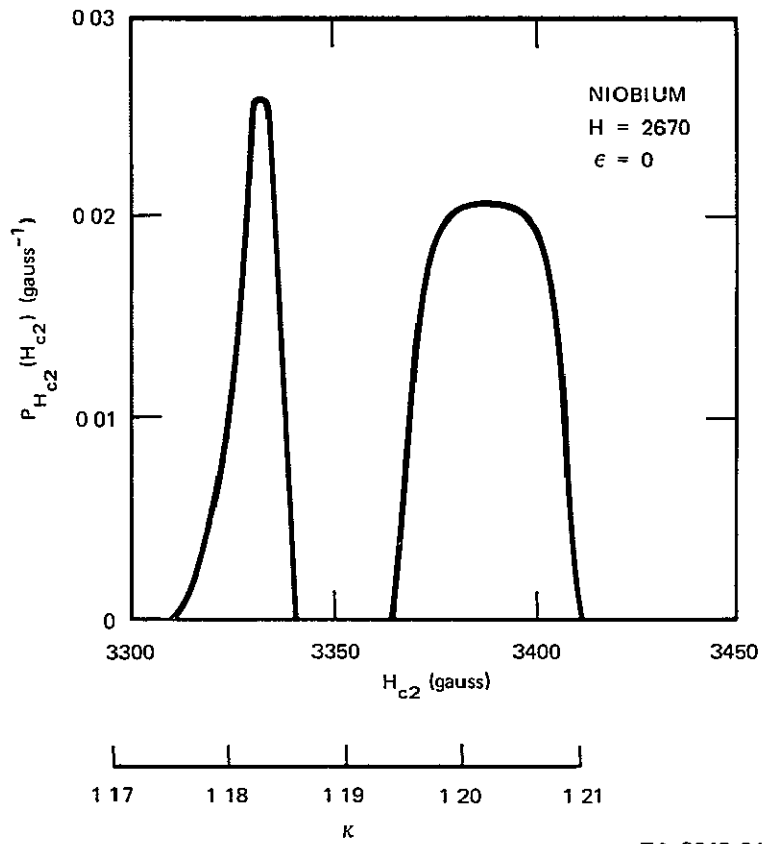
FIGURE 24 DISTRIBUTION IN $H_{c2}$ OR $\kappa$ IN AN ANNEALED NIOBIUM SAMPLE OBTAINED FROM SPECIFIC HEAT CAPACITY MEASUREMENTS IN HIGH FIELD The field was 2670 gauss

FIGURE 25 DISTRIBUTION IN $H_{c2}$ OR $\kappa$ IN A NIOBIUM
SAMPLE OBTAINED FROM SPECIFIC HEAT
CAPACITY MEASUREMENTS IN HIGH FIELD
The field was 2745 gauss The strain was 0 07

FIGURE 26    DISTRIBUTION IN $H_{c2}$ OR $\kappa$ OBTAINED FROM SPECIFIC
HEAT CAPACITY MEASUREMENTS AT HIGH FIELD    The
field was 2745 gauss    The strain was 0 20
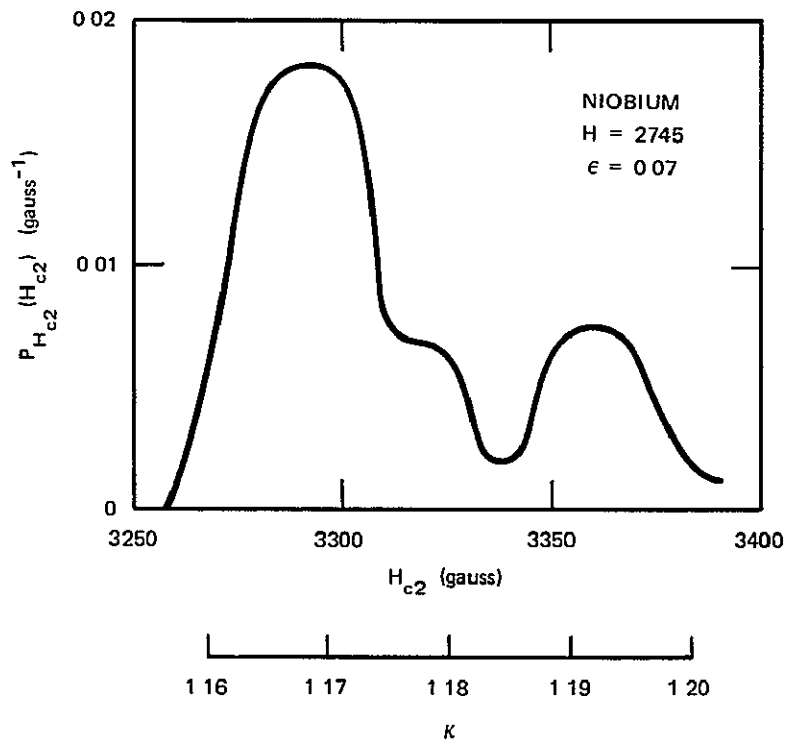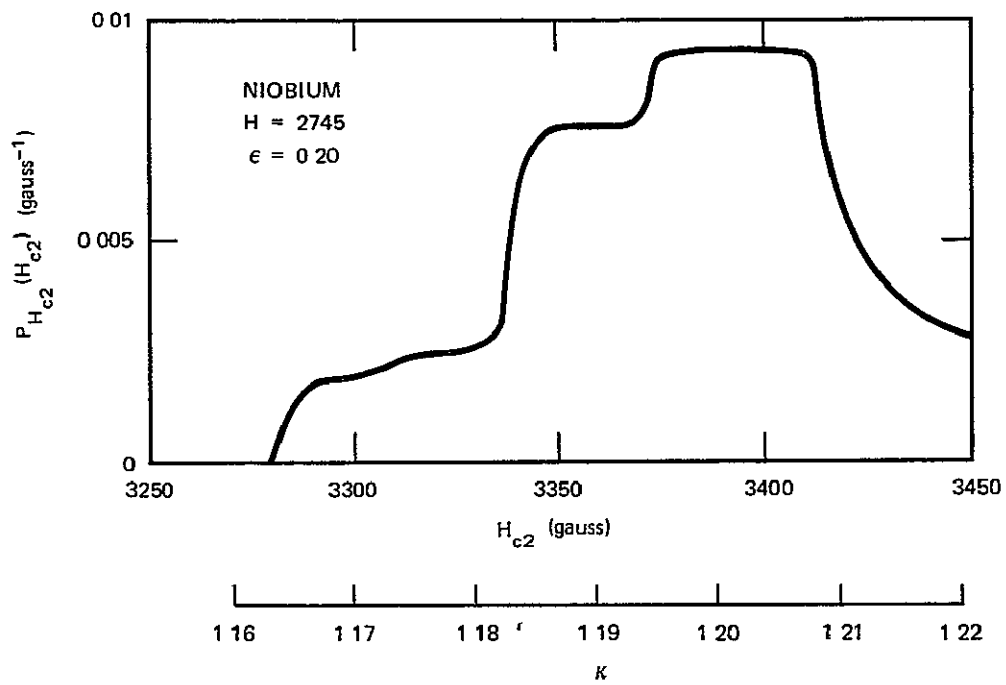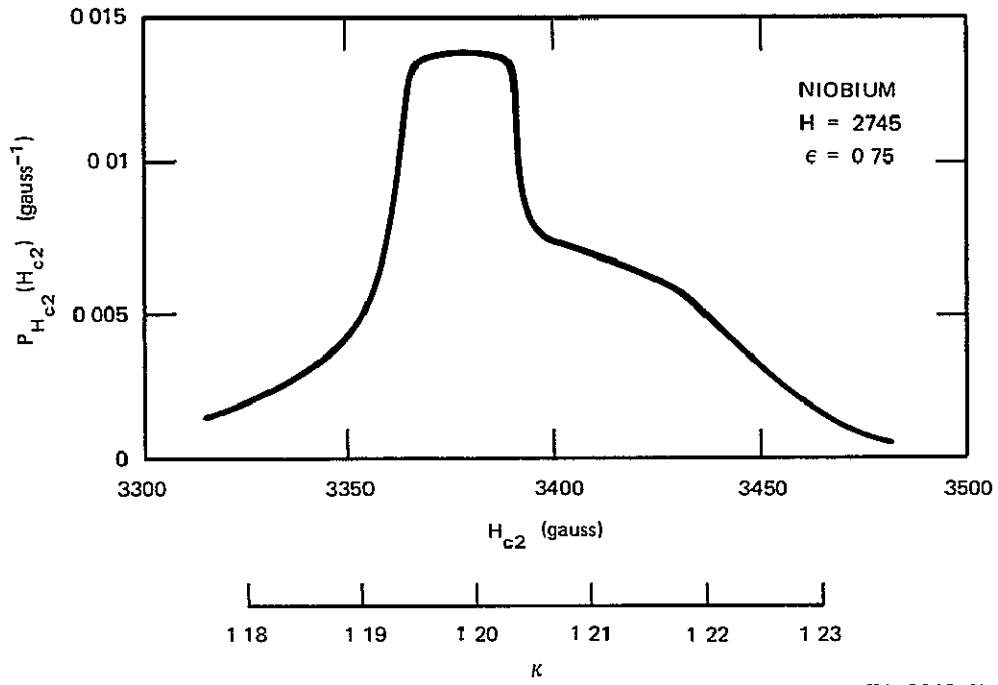
FIGURE 27    DISTRIBUTION IN $\kappa$ OBTAINED FROM SPECIFIC HEAT
CAPACITY MEASUREMENTS AT HIGH FIELD    The
field was 2745 gauss    The strain was 0 75

is less complicated in structure   The peak that remains corresponds to the highest $H_{c2}$ or $\varkappa$ peak in the annealed sample   Further, the lower $\varkappa$ material has disappeared and has been converted into a high $\varkappa$ distribution that extends about 5% above the value of $\overline{H}_{c2}$   The extension of the distribution at high strain toward a higher $\varkappa$ clearly represents improvement of the magnetic field properties of the material, as well as improvement in the pinning properties as discussed earlier

## Conclusion

Our major conclusion from the specific heat capacity data analysis is that the technique developed for the analysis of high resolution specific heat data has implications to the analysis and understanding of the metallurgy of superconducting materials that extend far beyond the particular samples analyzed in this report   There appears to be an opportunity for a detailed understanding of the metallurgy, and a characterization of the contribution of different types of imperfections and defects to probability distributions over the relevant parameters   We have observed in detail the tendency of imperfections to increase the transition temperature and $H_{c2}$ or $\varkappa$   We have observed also the strain induced broadening of the distributions in $T_o$ and $\varkappa$, causing a cutoff below the unstrained values of $\overline{T}_o$ and $H_{c2}$ and extending the tail of the distributions some considerable distance above $\overline{T}_o$ and $\overline{H}_{c2}$   These distributions clearly indicated how large strains can improve the temperature and magnetic field characteristics of superconductive materials

This analysis technique should be applied to practical materials such as superconducting magnet wire at various stages of manufacture to determine the effects of the manufacturing processes on the distributions of $T_o$ and $\varkappa$   Because our time and funds were depleted sooner than expected, we were unable to perform extensive metallurgical studies on the niobium samples   This would have enabled us to identify the types of

defects in the sample, and determine methods of improving the $T_o$ and $H_{c2}$ distributions    However, for practical assessment of materials we have provided a basis for completely characterizing superconducting materials by macroscopic specific heat measurements

In fact, the technique appears useful enough that $T_o$ and $H_{c2}$ or $\varkappa$ distributions should be treated as primary data for understanding the behavior of superconducting materials

Finally, the $T_o$ and $\varkappa$ distributions can be interpreted as the relative fraction of volume that has a particular $T_o$ or $\varkappa$    What we do not know is whether these changes in properties are concentrated in small regions of the sample or whether they are finely distributed throughout the sample in small clusters.  This question must be answered by detailed microscopic metallurgical examination

# BITTER PATTERN MEASUREMENTS

The purpose of the Bitter pattern experiments was to observe the distortion of the fluxoid lattice in imperfect type-II superconducting niobium resulting from the interaction of the fluxoid lattice with the defect structure of the material. For example, if the fluxoid lattice maintained its hexagonal symmetry, but showed a continuous variation in lattice parameter or fluxoid spacing, this could be related to a flux gradient Such flux gradients result from pinning, and direct observation on the scale attainable with this technique would allow correlation of these flux gradients with microscopic defect distributions The surface structure of the sample observed is of primary importance in that variations in the microscopic sample thickness would introduce flux gradients resulting from variation of the total free energy of the system with the sample thickness These observations were to act as a guide to calculations made using the theoretical model developed in this work

## Experimental Method

The method of observing the distribution of flux in type-I and type-II superconductors is a modified Bitter pattern technique The Bitter pattern technique was developed[29] to allow the observation of magnetic domain walls in iron, nickel, and cobalt In this technique, a colloidal suspension of small (less than 200-$\overset{\circ}{A}$ diameter) ferromagnetic particles is placed on the surface of a ferromagnetic material The particles experience a force when in the presence of an inhomogeneous magnetic field and are drawn to the points on the surface of the sample at which the magnetic field intensity is highest In this colloidal

57

suspension, the particles are free to move and distribute themselves in
a manner determined by the field intensity distribution at the sample
surface  By observing the variations in the density of the particles,
the spatial variation of the magnetic field (i e , the position of the
domain walls) can be determined.

This method has been applied also to investigations of the inter-
mediate state in type-I superconductors, using both ferromagnetic and
superconducting powders  This application has been reviewed by Livingston
and De Sorbo [30]  In these observations, the normal or the superconducting
state domains are delineated by the magnetic powders  More recently a
technique with which higher resolutions are possible has been reported [31]
This technique is similar to one developed independently at SRI.  It con-
sists of evaporating a ferromagnetic metal (iron, cobalt, or nickel) from
a refractory heater in a helium gas atmosphere onto a sample in the super-
conducting state  The ambient pressure is extremely important and de-
termines the resulting particle size  Fine particles with diameters down
to 80 Å can be produced in this manner at gas pressures between 0 5 and
1 0 torr  These particles are allowed to settle on the superconducting
surface and distribute themselves in a pattern determined by the local
magnetic flux density.  Individual fluxoids as well as the fluxoid lattice
in type-II materials have been observed by this technique.[32,33]

The resolution necessary for the observation of fluxoids is defined
by the value of the parameter $\varkappa$ from the GLAG theory and, therefore, by
the penetration depth and the coherence length  The spacing, d, of these
fluxoids in the hexagonal array is described in terms of the bulk magnetic
induction, B, and is given by $1/d^2 = qB/\varphi_0$, where q is a geometric factor
describing the packing density in the hexagonal array, and $\varphi_0$ is the flux
contained in a single fluxoid  For relatively pure niobium, having a
$\varkappa$ of 1.2 at 4 2°K, a fluxoid spacing of the order of 1,700 Å is expected

for inductions of approximately 700 G    This represents about 20 magnetic

particle diameters and allows sufficient resolution for observation of

individual fluxoids    This spacing increases as the magnetic induction,

B, decreases and larger spacings are possible with materials of higher

$\varkappa$ due to the resulting lower values of $H_{c1}$    In fact, spacings of the

order of 6,300 Å are predicted for inductions of the order of 50 G.

In the Bitter technique, particle agglomeration is necessary for

the observation of the distribution of the magnetic flux in the sample

The conditions for this to occur have been determined by Kittel[34] for

the case of a colloidal suspension of particles    He found that this dis-

tribution was field-dependent and given as $P(H) = \sinh (\mu H/kT)/(\mu H/kT)$,

where $P(H)$ is the particle density expected for a field H, $\mu$ is the mag-

netic moment of a particle, k is Boltzmann's constant, and T is the ab-

solute temperature    Analysis of this equation shows that usable particle

densities are expected when $(\mu H/kT) \geq 3\ 0$    For iron particles of 80-Å

diameter at a temperature of $4^{\circ}$K, this requires the local field to be

larger than about 4 G    This condition is met since the field at the

fluxoid core is greater than the applied field.


## Experimental Apparatus and Procedures

The experimental apparatus was designed so that samples at tempera-

tures between 2.0 and 5 $0^{\circ}$K could be studied.    The apparatus generally

consisted of a vacuum-tight thin-wall stainless tubular probe 24 in.

long X 1-1/4 in    diam    that was isolated from the liquid helium bath

The sample was mounted in this probe    The probe was filled to one at-

mosphere pressure with helium gas after pumping and purging three times.

It was then inserted into the liquid helium bath after cooling by immer-

sion in liquid nitrogen.    The probe fit (with 0 020-in    clearance) into

a superconducting niobium wire solenoid (458 gauss/A)

A schematic drawing of the inserted probe is shown in Figure 28
The sample (typically a disc 0 250-in diam and 0 005 to 0 020-in. thick)
is mounted at (1) and is thermally grounded to an OFHC copper sample
mounting block (7). This block can be removed from the end of the probe
for mounting and examination of the sample  A vacuum tight seal is made
using a sheared indium gasket (8)  The sample is optically shielded (2)
from the evaporation source (3). The evaporation source (3) is mounted
on the end of two 0.150-diam  stainless steel rods (4) that act as power
leads for the evaporation source and are isolated from the probe walls
(6) by teflon spacers (12)  The sample is positioned at the center of
the magnet. The whole system is immersed in liquid helium contained in
a double-wall glass dewar (10).

A typical experimental sequence is as follows  The sample is posi-
tioned as described above  The helium gas pressure in the probe is re-
duced to 250 $\mu$  This initial pressure was determined empirically and is
the pressure necessary for particles of approximately 200 Å to be formed
during the evaporation. The sample is allowed to sit in a constant mag-
netic field for one hour to ensure complete deposition of the ferromagnetic
powder so that no erroneous patterns will be observed because of powder
deposition during removal of the probe from the liquid helium. The sample
is then removed from the liquid helium and allowed to warm to room temper-
ature over a period of three hours  The sample is removed and a 500-Å
carbon layer is deposited. Subsequent observations are made on samples
in this configuration

Experimental Results

A total of 19 experiments were performed, eleven of which are listed
in Table 2  The remaining eight are not described in detail since they
were directed toward empirical definition of the experimental conditions
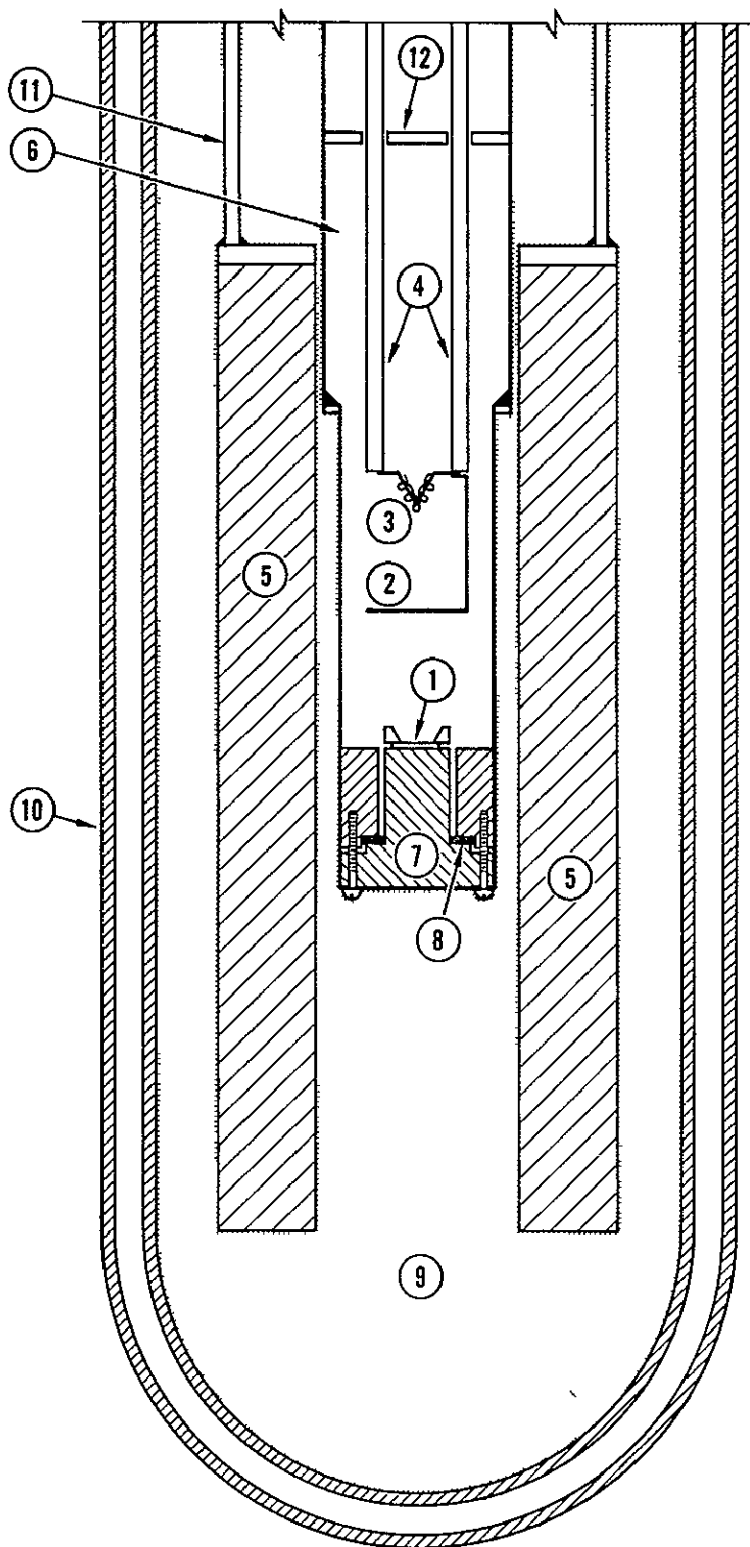
(1) SAMPLE

(2) OPTICAL HEAT SHIELD

(3) COBALT WRAPPED
TUNGSTEN FILAMENT
EVAPORATION SOURCE

(4) STAINLESS STEEL POWER
LEADS AND EVAPORATOR
SUPPORT

(5) NIOBIUM WIRE SUPER-
CONDUCTING MAGNET
(458 gauss/amp)

(6) STAINLESS STEEL THIN
WALL EVAPORATION
CHAMBER

(7) ANNEALED O F H C
THERMAL GROUND
SAMPLE MOUNTING
BLOCK

(8) INDIUM GASKET

(9) LIQUID HELIUM

(10) DOUBLE WALL
GLASS DEWAR

(11) MAGNET SUPPORT
STRUCTURE

(12) TEFLON CENTERING
PIECES

TA-8043-10

FIGURE 28   EXPERIMENTAL APPARATUS FOR BITTER PATTERN MEASUREMENTS

61

Table 2

BITTER PATTERN EXPERIMENTS PERFORMED ON DEFORMED AND ANNEALED NIOBIUM

| Experiment Number | Temperature ($^\circ$K) | Field (gauss) | Deposition Conditions | | Pressure ($\mu$) | Observations | |
|---|---|---|---|---|---|---|---|
| | | | Time (sec) | Current (A) | | Optical | Electron Microscope |
| 8043-1<br>$\epsilon = 0$ | 4 2$^\circ$ | 1,000 | 0 4 | 55 | 200-<br>1,500 | X | X |
| 8043-2<br>$\epsilon = 0\ 20$ | 4 2 | 1,000-<br>500 | 4 | 55 | 200-<br>1,100 | X | X |
| 8043-3<br>$\epsilon = 0\ 20$ | 4 2 | 1,000-<br>500 | 4 | 60 | 200-<br>350 | X | X |
| 8043-4<br>$\epsilon = 0\ 75$ | 4 2 | 1,500-<br>500 | 4 | 60 | 215-<br>2,000 | X | X |
| 8043-5<br>$\epsilon = 0\ 07$ | 4 2 | 1,000-<br>500 | 4 | 60 | 220-<br>700 | X | X |
| 8043-6<br>$\epsilon = 0\ 07$ | 4 2 | 1,000-<br>800 | 4 | 60 | 230-<br>750 | X | X |
| 8043-7<br>$\epsilon = 0\ 20$ | 4 2 | 1,000-<br>800 | 5 | 60 | 225-<br>400 | X | X |
| 8043-8<br>$\epsilon = 0$ | 4 2 | 1,000-<br>500 | 5 | 60 | 225-<br>750 | X | X |
| 8043-9<br>$\epsilon = 0\ 75$ | 4 2 | 1,000-<br>500 | 5 | 60 | 200-<br>400 | X | X |
| 8043-10<br>$\epsilon = 0$ | 4 2 | 750 | 7 | 60 | 200-<br>700 | X | X |
| 8043-11<br>$\epsilon = 0\ 75$ | 4 2 | 1,000-<br>0 | 7 | 60 | 180-<br>350 | X | X |

necessary to produce the correct helium gas pressure in the sample probe and of the evaporation conditions necessary to produce the correct amount of powder without unnecessary heating of the samples.

Samples deformed from 0 to 75% by rolling were examined  Typically, the external field was raised to 800 to 1,000 gauss and then reduced to approximately 500 to 800 gauss.  This sequence was used so that stable flux distributions were established in the samples and so that the trapped flux density in the samples exceeded the external field.  The powder is attracted to the sample and controlled experiments are possible.

All samples listed in Table 2 were examined using both electron and optical microscope techniques, e.g , during optical microscopy, observations were made of sample 8043-5, a pure niobium sample deformed 7% by rolling.  A steady applied field of 500 gauss was maintained on the sample after cycling the field to 1,000 gauss  Since the lower critical field of high purity niobium at 4 2$^\circ$K is nearly 1,500 gauss, the sample was never fully in the type-II state and the mixed state structure was defined poorly.  The structure of the sample is shown in the low magnification micrograph of Figure 29  Essentially, no microscopic structure is obtainable in this picture

In Figure 30, the flux distribution at the sample edge is shown. A quasi-intermediate state structure is apparent in this figure with the regions of high flux density lying nearly parallel to the sample radius. This structure is consistent with flux distributions obtained in other type-II materials at fields less than the lower critical field

In Figures 31, 32, and 33, the flux distributions near the center of the sample are shown.  Two specific characteristics are apparent. First, the flux distribution is nonuniform, but locally isotropic  What appear to be flux spots of nearly uniform size are shown.  These consist of high densities of individual quantum fluxoids.  The local field
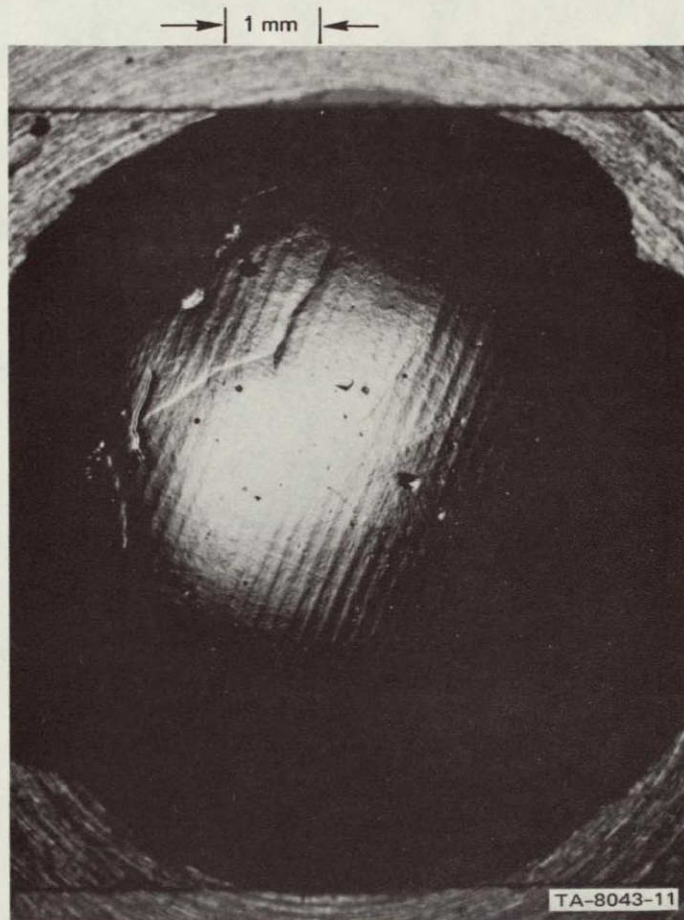
FIGURE 29    MICROGRAPH OF SAMPLE STRUCTURE
(SAMPLE 8043-5)

100 μ

TA-8043-12

FIGURE 30    FLUX DISTRIBUTION AT THE SAMPLE
EDGE.   Lines of high flux density show
a quasi-intermediate state structure.

→| 100 μ |←

TA-8043-13
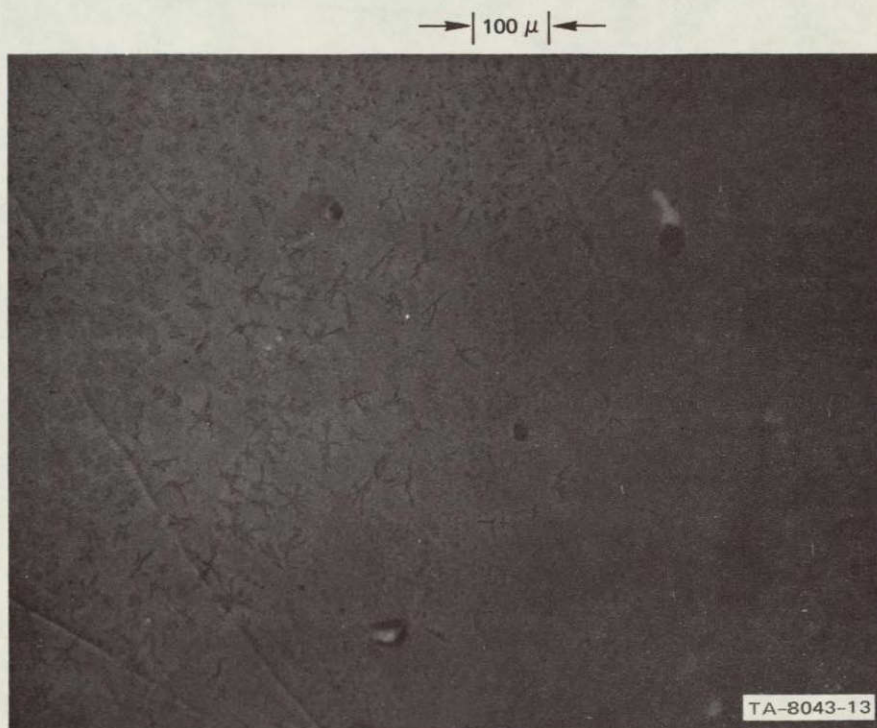
FIGURE 31    FLUX SPOTS AND REGIONS OF RATHER HIGH
             FLUX DENSITY NEAR THE CENTER OF THE
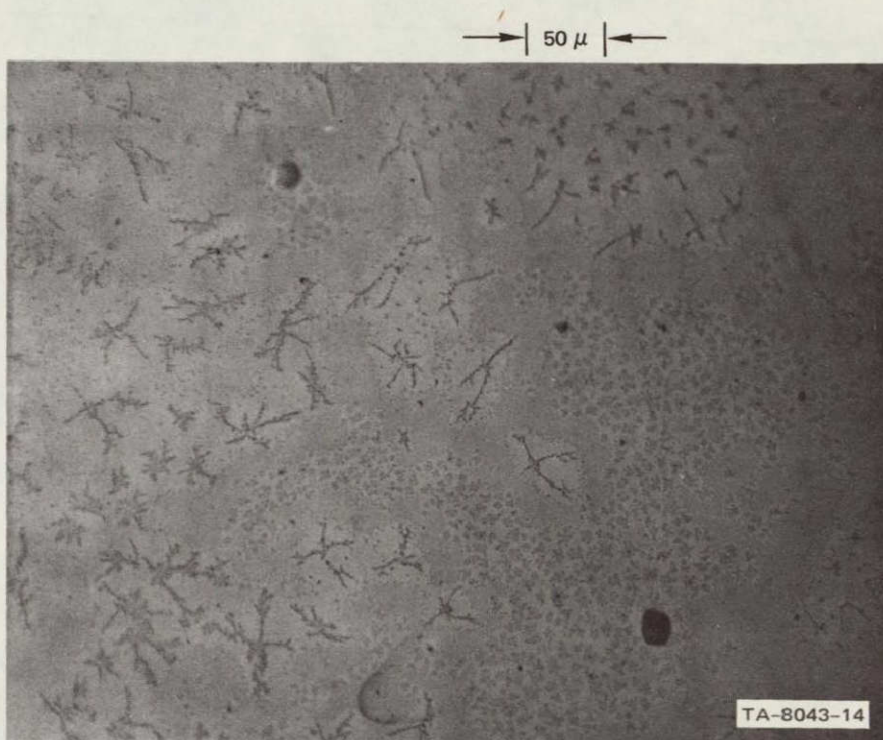             SAMPLE

⟶ | 50 μ | ⟵

TA-8043-14

FIGURE 32     FLUX DISTRIBUTION AT THE SAMPLE
CENTER

→| 20 μ |←

TA-8043-15

FIGURE 33    FLUX DISTRIBUTION AT CENTER OF SAMPLE.
The regions of high flux density have a structure
that is not fully resolvable in this micrograph.

intensity in these flux spots is of the order of 700 gauss, the equili-
brium induction for fields just above the lower critical field of nio-
bium  Therefore, the fluxoid spacing expected is of the order of 2,000 Å
which is beyond the resolution of optical microscopes.  This is shown in
Figure 33 where obvious, though unresolvable, structure is seen within
the individual flux spots  At a magnification of 500X, 2,000 Å is equal
to 0.1 mm  Therefore, it is likely that individual fluxoids may be shown
in this micrograph because of some randomness in the powder deposition,
but the detailed structure cannot be resolved.

The carbon film was stripped from this sample using standard repli-
cation techniques and observed in the electron microscope in transmission
Essentially none of the deposited powder was removed and, therefore, no
data were obtained  This problem was encountered in all the samples
investigated, and although the scant optical observations indicated that
interesting patterns were formed, we were unable to observe them in
detail.

The experimental problem of removing the deposited powder from the
sample surface for observation in the electron microscope limited the
observations in this work.  Several techniques typically used to aid in
the removal of carbon films from sample surfaces were tried  These in-
cluded etching, electropolishing, and deposition of a parting layer before
the formation of the powder pattern.  None of these was successful, al-
though the inclusion of a parting layer did show indications of leading
to a solution to the problem

Conclusion

A series of experiments directed toward the direct observation of
flux distributions in type-II superconductors by a modified Bitter pat-
tern technique have been conducted  The purpose of these experiments

69

was to observe quantum fluxoid distributions in imperfect type-II super-conductors and to correlate imperfections in the fluxoid lattice with defect structure

Although optical micrographs indicated that several interesting Bitter patterns were formed on the niobium samples, the inability to strip the powder from the sample surface prevented us from observing these patterns with the electron microscope  We were unable to resolve this problem with the time and funds available

# CONCLUSIONS

- The theoretical model formulated in this project is a good approximation to the Ginzburg-Landau theory and is mathematically tractable

- Flux pinning arises from a variety of metallic defects, each of which contributes to the critical current density in a different way. Three types of pinning were analyzed

- The peak effect was found to be caused by small dispersed inclusions of material with a $\varkappa$ value higher than that of the host material

- A method for analysis of the $\varkappa$ and $T_0$ distributions in superconductors caused by deformation was formulated  The method uses experimental specific heat measurements. Using this analysis, distributions of $\varkappa$ and $T_0$ in annealed and deformed niobium samples were determined

- Bitter patterns showing the location of fluxoids in pure annealed and pure deformed niobium were formed. Problems associated with replicating these patterns precluded observing the patterns in detail using electron microscopic techniques

# RECOMMENDATIONS

• The theoretical model developed in this program provides a
simple, accurate means of calculating the properties of
type-II superconductors and should be explored in more detail
The results of the flux pinning calculations should be com-
pared with experiments on carefully controlled samples  The
peak effect analysis should be checked experimentally by
introducing a microscopic dispersion of a second material
with a $\varkappa$ slightly higher than that of the host material
If the predictions can be verified, a method of controlling
the current density at high fields would result

• The technique for analysis of specific heat data developed
in this program should be applied to superconducting wire
and other practical materials  The technique can aid
considerably in the understanding of the relationship between
the macroscopic performance and the microscopic metallurgy
of superconducting materials

• The Bitter pattern technique used shows promise of providing
a direct measure of the pinning forces exerted on fluxoids
by different types of pinning centers.  This information would
be valuable in assessing the accuracy of theoretical models
of the type developed in this program  This technique should
be developed to its full potential.

CITED REFERENCES

1   A. A. Abrikosov, Zh  Eksperim  ı  Teor. Fiz. $\underline{32}$, 1442 (1957)
    (English Translation   Soviet Phys – JETP $\underline{5}$, 1174 (1957)

2   L  P. Gor'kov, Zh Eksperim  ı. Teor  Fiz  $\underline{36}$, 1918 (1959)
    (English Translation   Soviet Phys – JETP $\underline{9}$, 1364 (1959)

3   V  L  Ginzburg and L. D  Landau, Zh  Eksperim  ı  Teor  Fiz  $\underline{20}$,
    1064 (1950)

4.  F. London, Superfluids, Vol. 1, Dover Publications, Inc., New York,
    1960

5   J. Friedel, P  G  DeGennes, J. Matricon, Appl  Phys  Letters $\underline{2}$,
    119 (1963), P. G  DeGennes and J. Matricon, Rev  Mod. Phys $\underline{36}$, 45
    (1964)

6   M. Tinkham, Phys. Rev  $\underline{129}$, 2413 (1963)

7   P  M. Marcus, in Low Temperature Physics LT9 (J. Daunt, D  Edwards,
    F. Milford, et al., eds ), Plenum Press, Inc , New York, 1965, 550

8   H. T  Coffey, Phys  Rev  $\underline{166}$, 447 (1968)

9.  W  DeSorbo, Phys  Rev  $\underline{132}$, 107 (1963), Phys. Rev  $\underline{134}$, A1119 (1964)

10  J  D  Livingston, J. Appl  Phys. $\underline{34}$, 3028 (1963), Rev  Mod. Phys.
    $\underline{36}$, 54 (1964), Appl  Phys  Letters $\underline{8}$, 319 (1966)

11  J. P. McEvoy, Jr , R. F. Decell, and R. L. Novak, Appl  Phys
    Letters $\underline{4}$, 43 (1964)

12. G  W. Cullen and R  L  Novak, Appl. Phys  Letters $\underline{4}$, 147 (1964), with
    J  P  McEvoy, R  C. A. Rev. $\underline{25}$, 479 (1964)

13  P. S  Swartz, H. R  Hart, and R  L  Fleischer, Appl. Phys  Letters
    $\underline{4}$, 71 (1964)

14. H. T. Coffey, E. L. Keller, A Patterson, and S. H Autler, Phys. Rev. 155, 355 (1957), Appl Phys. Letters 9, 270 (1966)

15 K. J Gifkins, C Malseed, and W. A. Rachinger, Script Metallurgica 2, 141 (1968)

16 A M Campbell, J E Evetts, and D Dew-Hughes, Phil Mag 18, 313 (1968)

17 D. Kramer and C G Rhodes, J Inst Metals 94, 261 (1966)

18. G R Love and C. C. Koch, Appl Phys Letters 14, 250 (1969)

19 C C Koch and G R Love, Trans. Metal Soc 245 (1969)

20 J E Evetts, Phys Rev B, 2, 95 (1970)

21 B B Goodman, IBM J. Res. Develop 6, 63 (1962)

22. W. H. Kleiner, L. M Roth, and S H. Autler, Phys Rev 133, A1226 (1964)

23. G. R Love, Phil. Mag 21, 1003 (1970)

24 E. W Urban, Ph D dissertation, University of Alabama, 1970

25 A. C. Van Vijfeijken, On the Theory of Vortices in Type-II Super-conductors, Ph D dissertation, University of Amsterdam, 1967

26 P. F. Sullivan and G. Seidel, Phys Rev. 173, 679 (1968)

27 T. W Barbee, Jr., Phys Status Solidi 31, 535 (1969)

28 D. K. Finnemore, T F Stromberg, and C A. Swenson, Phys Rev 149, 231 (1966)

29 R Carey and E D Issac, Magnetic Domains and Techniques for Their Observation, Academic Press, New York, 1966

30 J D. Livingston and W DeSorbo, Gen. Elect Tech. Rept No 66-C-388, 1966

31 U Essman and A Traubel, Phys Status Solids 20, 95 (1967)

32   U  Essman and A. Traubel, Phys. Letters 24A, 526 (1967)

33   N  V  Sarma, Phys  Letters 25A, 315 (1967)

34   C. Kittel, Phys  Rev  76, 1527 (1949)